

pubs.acs.org/acscatalysis Research Article

Identification of a Selectivity Descriptor for Propane Dehydrogenation through Density Functional and Microkinetic Analysis on Pure Pd and Pd Alloys

Ranga Rohit Seemakurthi, Griffin Canning, Zhenwei Wu, Jeffrey T. Miller, Abhaya K. Datye, and Jeffrey Greeley*



Cite This: ACS Catal. 2021, 11, 9588-9604



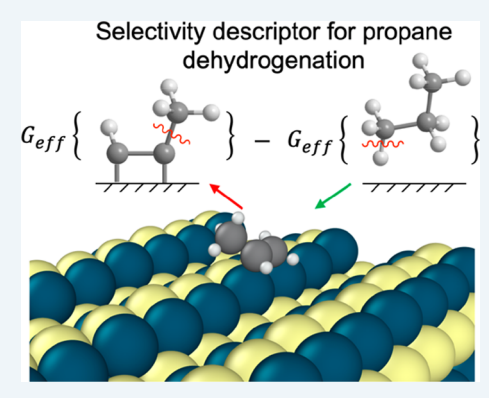
ACCESS

Metrics & More

Article Recommendations

Supporting Information

ABSTRACT: First principles periodic density functional theory (DFT) calculations, in conjunction with detailed microkinetic modeling and experimental characterization, are employed to elucidate the structure sensitivity and identify key selectivity descriptors for nonoxidative propane dehydrogenation (PDH) on intermetallic alloys. A comprehensive theoretical treatment of 1:1 PdIn surfaces demonstrates that the Pd-terminated steps have 5 orders of magnitude higher rates than do the (110) terraces, with nearly complete selectivity to propylene formation. Pure Pd steps and terraces, in contrast, have considerably lower propylene selectivity and higher coverages of adsorbed intermediates, suggesting that Pd may experience more coking and reduced lifetimes compared to the alloys. A degree of rate and selectivity control analysis on the optimized microkinetic model demonstrates that propane C—H bond scission to yield 1-propyl is the most kinetically relevant step for propylene formation, while the C—C bond breaking barriers are important for byproduct formation. From these analyses, a simplified rate expression is derived for the step



surface of the alloy, leading to the identification of a selectivity descriptor expressed in terms of effective free energy barriers of the rate controlling transition states, propane C–H bond breaking, and propyne C–C bond breaking. This descriptor is subsequently generalized to evaluate the propylene production selectivities for a series of Pd-containing alloys. The results show enhanced agreement with experimentally measured selectivity trends compared to traditional selectivity descriptors, suggesting a general strategy for identification of highly selective, nonoxidative PDH alloy catalysts.

KEYWORDS: alloys, density functional theory, propane dehydrogenation, selectivity descriptor, catalysis

■ INTRODUCTION

Recent increases in shale gas production have led to shifts in steam cracking feeds from naphtha to ethane, resulting in abundant ethylene production. However, propylene, which is a side product of naphtha steam cracking, is produced to a far lesser extent during the ethane steam cracking process.2 Interest in on-purpose production of propylene has, therefore, increased significantly,3 with nonoxidative dehydrogenation of propane (PDH) being a promising strategy. Nevertheless, the endothermic nature of propane to propylene conversion necessitates the use of high temperatures which ultimately leads to deep dehydrogenation, hydrogenolysis (C-C bond breaking), and coke formation. Intermetallic alloys of Pt, 4-14 Pd, 15-18 and Ni, 19 with promoters such as Sn, Zn, Fe, In, and Ga, have shown promise in enhancing selectivity and reducing byproduct formation compared to their pure metal counterparts, but improvements are still needed. This imperative, in turn, motivates development of a fundamental understanding of the reaction mechanism, including structure-property relationships, on the alloy surfaces.

Density functional theory (DFT)-based studies have analyzed ethane^{20–25} and propane dehydrogenation^{26–34} selectivity trends across pure Pt and Pt alloys. Computational studies of PDH have considered Pt and industrially used Pt₃Sn alloys,^{26–29} wherein the difference between the propylene binding energy and the propylene C–H bond activation barrier was introduced as a selectivity descriptor to evaluate the relative rates of propylene desorption compared to unselective deep dehydrogenation.^{27,28} Using this descriptor, the researchers rationalized the experimentally observed increase in propylene selectivity on Pt₃Sn as compared to Pt. More recently, in-depth microkinetic studies on Pt surfaces concluded that the initial C–H bond activation step in

 Received:
 April 27, 2021

 Revised:
 June 28, 2021

 Published:
 July 16, 2021





propane, C-H bond activation in propylene, 30,34 and C-C bond breaking in propyne (CH₃CCH*)³⁰ are kinetically relevant steps in PDH. Gong and co-workers³¹ have also carried out a trends-based study of PDH chemistry across a series of Pt₂X(111) alloy surfaces. By evaluating the first dehydrogenation barrier of propane, which was used as a proxy for PDH activity, in addition to a selectivity descriptor comparing the desorption and dehydrogenation barriers of propylene, the authors demonstrated that there exists a negative correlation between these activity and selectivity descriptors and that Pt₃In represents a useful trade-off between these two reactivity measures. Recent work from Miller, Greeley, and co-workers³⁵ combined experiments and DFT calculations to demonstrate that trends in propylene selectivity across five Pd-containing alloys of variable composition can be reasonably explained by both the aforementioned selectivity descriptor and the C-C bond breaking barriers of deeply dehydrogenated intermediates. In general, computational studies have been largely consistent with experimental studies of PDH, which, as mentioned above, have largely shown increased selectivity of alloys compared to pure Pd and pure Pt. 2,6,10,16 However, the selectivity descriptors employed in these studies remain generally empirical in nature, and there exist strong scientific and practical motivations to rigorously evaluate the kinetic foundations of these selectivity descriptors across a range of Pt- and Pd-based alloys.

In addition to the elemental identity of promoter elements in the alloys, the structure sensitivity of C-H and C-C bond breaking reactions^{27,36–38} can affect PDH rates and selectivity on both pure metal and alloy catalysts. Experimental studies of PDH from De Chen et al. 38,39 demonstrated that, by increasing the size of Pt particles, the amount of coke formation decreased while the selectivity toward propylene increased, suggesting that increased edge and corner density correlates with lower propylene selectivity. To provide a molecular perspective on how surface defects affect catalytic activity and coke formation, an extensive computational reaction network analysis, including deep dehydrogenation and C-C bond breaking pathways, was performed on both (111) and (211) facets of Pt. 34,40 The results demonstrated that C-C bond breaking occurs in deeply dehydrogenated species such as propyne, leading to the formation of atomic carbon, which is a possible precursor for coke formation. Furthermore, through the inclusion of step surfaces of Pt in the microkinetic model, the authors were able to explain experimentally observed decreases in propylene selectivity with increasing H₂/C₃H₈

Finally, it should be noted that the quantity of promoter elements in alloys can influence the properties of PDH catalysts, and 1:1 alloys of both Pt and Pd have recently been shown to exhibit similar catalytic performance⁵ to, and in some cases even greater selectivity than, the commonly studied 3:1 alloys.35 The present study begins with a detailed analysis of one such alloy, a 1:1 PdIn intermetallic, which has been shown to convert propane to propylene with much higher selectivity than pure Pd. 15,35 DFT calculations, in conjunction with microkinetic modeling, are used to study the complete PDH reaction network on both steps and terrace surfaces of the alloy, and a similar analysis is subsequently performed on pure Pd. The results demonstrate that Pd-terminated steps on the PdIn alloy exhibit approximately 5 orders of magnitude higher activity than the PdIn terraces, while both steps and terraces have very high selectivity compared to corresponding structures on Pd. The selectivity trends are traced to a competition between rates for propyne C–C bond breaking and propane C–H bond breaking steps, which in turn suggest a modified descriptor for PDH selectivity on alloy surfaces. Comparison to both the traditional PDH selectivity descriptor, which compares propylene binding energies and dehydrogenation barriers, and experimental results demonstrates that the new descriptor captures selectivity trends across a wide range of alloy surfaces with high fidelity. The analysis may form a basis for future studies to identify alloy catalysts with enhanced selectivity for PDH.

METHODS

Computational Methods. Periodic density functional theory (DFT) calculations are performed with the Vienna Ab-initio Simulation Package (VASP),^{41–44} where the Kohn– Sham equations are solved self-consistently using the Perdew, Burke, and Ernzerhof functional (PBE)^{45'} with the Projector Augmented Wave (PAW) method.^{46,47} Selected adsorption calculations are also performed with the optPBE⁴⁸ and BEEFvdW⁴⁹ functionals to evaluate the effect of vdW interactions on the adsorption energetics (SI section 16). The calculated bulk lattice constants for bcc PdIn and fcc Pd are 3.30 and 3.94 Å, respectively, as compared to experimental values of 3.21 and 3.87 Å. 50,51 To model the bcc PdIn(110) surface, a 2 × 3 × 5 unit cell is used, while for fcc Pd(111), a $3 \times 3 \times 5$ unit cell is selected. To evaluate the structure sensitivity of PDH on PdIn, both Pd-terminated and In-terminated (210) steps with unit cells of $1 \times 3 \times 7$ are evaluated. Additionally, a (321) step, where the edge contains both Pd and In in equal proportions, with a $(2 \times 2 \times 5)$ cell, is examined. Finally, on pure fcc Pd, a (211) surface with a $3 \times 3 \times 5$ lattice is employed. A planewave energy cutoff of 400 eV is used with a $3 \times 3 \times 1$ kpoint set for all surfaces except the (321) step. Due to the larger unit cell size of the latter surface, a $2 \times 2 \times 1$ k-point set is employed. The Methfessel-Paxton scheme⁵² is used with an energy smearing of 0.2 eV to determine the partial electron occupancies. Adsorbates are relaxed until the forces are less than 0.02 eV/Å². These values are confirmed to converge the adsorption energies to within 0.05 eV. The slabs are separated in the z direction with a vacuum spacing of 20 Å. Spin polarization is not included in the calculations, with the exception of alloys containing naturally magnetized elements (Pd₃Fe and Pd₃Mn, more information in SI section 17), and dipole corrections are applied in the z direction to cancel out the net dipole moment on the surface. For density of states calculations, a tighter convergence criterion, using a higher energy cutoff energy of 520 eV and a gamma-centered 9 × 9 × 1 k-point grid, are employed with Blöchl corrections.

CatKit, ⁵³ a graph theory based algorithm, is used to identify all the possible adsorption configurations for monodentate and bidentate adsorbates. The binding energies are then calculated for all the identified configurations, and the energy of the most stable configuration is reported (Tables S4–S9). On all surfaces, adsorbed H is assumed to be in quasi-equilibrium with the gas phase H₂, since the standard free energy of desorption is negative on all the surfaces and since overbarriers for H₂ formation are small. Adsorption energies for reaction intermediates are calculated as formation energies referenced to stoichiometrically appropriate amounts of the relevant closed shell gas phase species, propane and H₂ (this formalism avoids the calculation of gas phase energies of radical species):

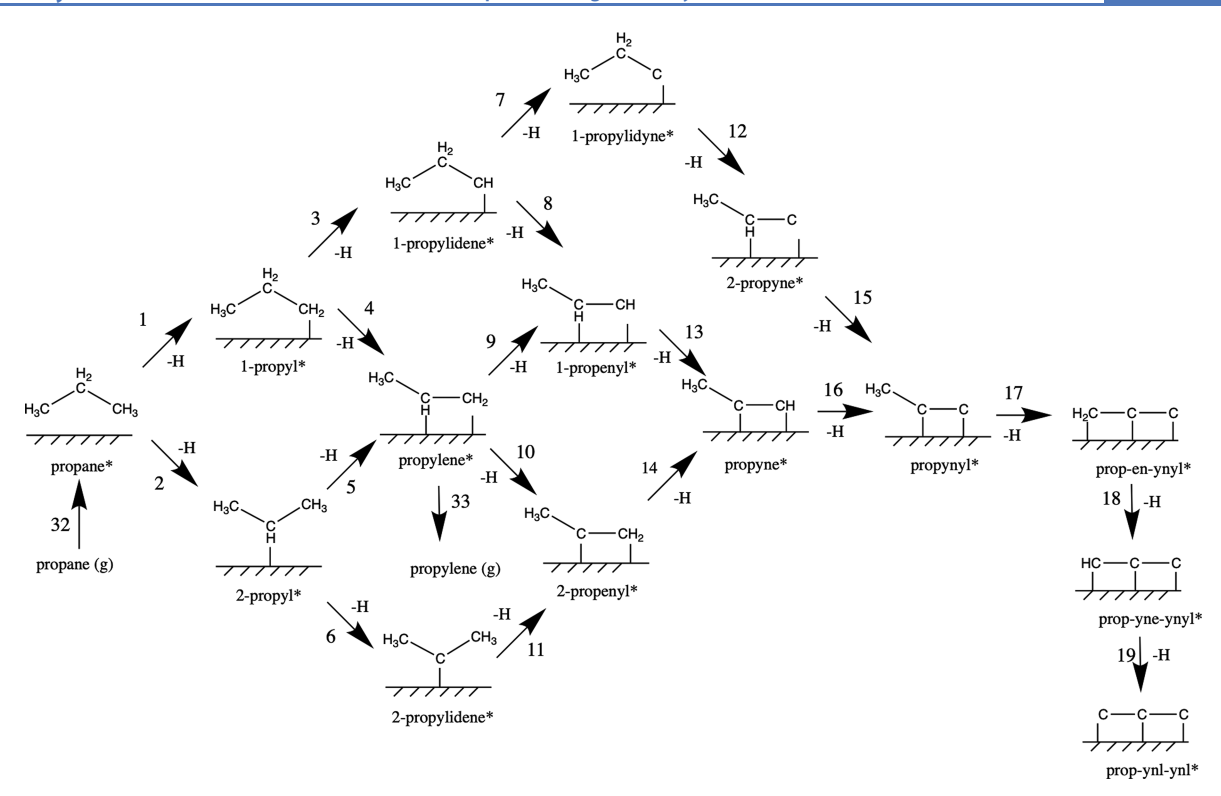


Figure 1. Detailed reaction network for propane and propylene (C_3) dehydrogenation pathways.

$$E_{\rm ads}({\rm C_3H_x}) = E_{{\rm C_3H_x/surface}} - E_{\rm surface} - E_{{\rm C_3H_8}} + 0.5 \times (8 - x) \times E_{\rm H_2}$$
 (1)

It is known that GGA functionals⁵⁴ do not well describe double and triple bonds in the gas phase due to the delocalized nature of these bonds. The gas phase energies of the alkene and alkyne molecules have therefore been modified to match the NIST reaction energies of formation from the respective alkanes (Table S3). The corrections are on the order of 0.1–0.2 eV for alkenes, while for alkynes, they are somewhat larger, at 0.2–0.3 eV. More details regarding the gas phase energetics and their corrections using NIST energetics can be found in SI section 2.

Activation barriers are calculated using the Climbing Image Nudged Elastic Band (CINEB) method, using both the first and second order approaches (Quick-Min, LBFGS, and dimer), developed by Henkelmann and co-workers. The initial images between the initial state and final state are generated using the Image Dependent Pair Potential (IDPP) method. An average of six to eight images are used for the CINEB calculations.

For all adsorbates, the standard free energy at 873 K is determined using the formula given in eq 2, which involves calculation of zero point energy (ZPE) and standard state entropy corrections, in addition to the DFT-calculated binding energies:

$$G^0 = E + ZPE - TS^0 \tag{2}$$

Harmonic vibrational states are used for the ZPE calculations, while for adsorbate entropies, a mode decomposition analysis is employed. In this scheme, the vibrational modes that have frequencies greater than 150 cm⁻¹ are treated as harmonic oscillators, while frequencies less than this cutoff are treated as either a hindered translator or rotor; the jmol software⁶⁰ is

used to distinguish between the translator and rotor modes. The partition functions for the hindered translator and rotor are taken from Sprowl et al., 61 and the associated diffusion or rotation barriers are determined using additional CINEB calculations. Transition state entropies are approximated by the corresponding initial or final state entropies, depending upon whether the TS is closer to the initial or final state on the NEB reaction coordinate (early or late transition state, respectively). Additionally, for the transition states which had a significant degree of rate control toward gas phase products, the entropy corresponding to the imaginary frequency is subtracted from the corresponding initial or final state entropy. Additional details about calculation of entropies for specific adsorbates and transition states are provided in SI section 5.

For the microkinetic analysis, a total of 52 surface reactions and seven adsorption/desorption steps involving 39 surface species are considered. The model is run as a CSTR at a temperature of 873 K and a pressure of 1 atm. The reactor dimensions and volumetric flow rates (Table S18) are chosen to match experimental conditions, 15,35 while the catalyst surface area is varied to adjust the conversion of propane. Further information regarding the details of the microkinetic model can be found in the Supporting Information (SI section 12). For the base case, the feed mole fractions are 2.5% C_3H_8 , 2.5% H_2 , and remainder Ar. The selectivity reported is based on the molar flow rate of products exiting the reactor (eq 3). Finally, the degree of rate control for each of the gas phase products (X_{RC_gi}) and selectivity control ($X_{SC_{C3H6}i}$) for propylene formation are estimated using eqs 4 and 5:

Selectivity
$$(S_{C_3H_6})$$

$$= \frac{n_{C_3H_6}}{n_{C_3H_6} + n_{C_2H_6} + n_{CH_4} + n_{C_2H_4} + n_{C_2H_2}}$$
(3)

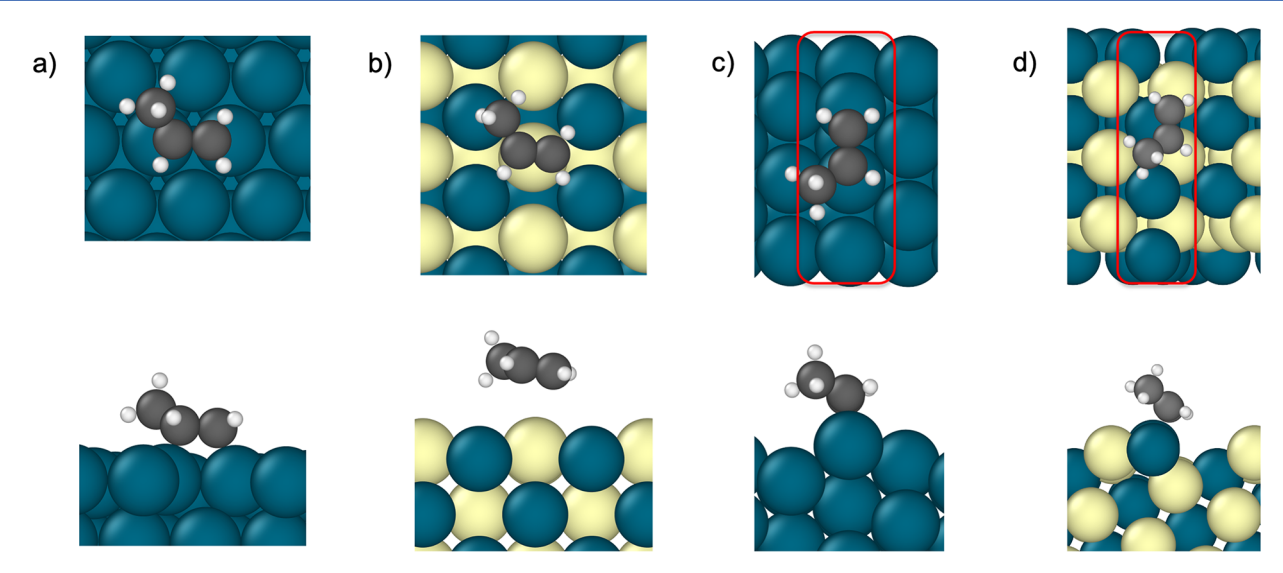


Figure 2. Top and side views of the most stable binding configurations of 1-propyl on (a) Pd(111), (b) PdIn(110), (c) Pd(211), and (d) Pd-step(210)_PdIn. The rectangle marked in red in c and d indicates where the step edge is located.

$$X_{\text{RC}_g,i} = \left(\frac{\partial \ln r_g}{\partial \ln k_i}\right)_{k_{j\neq i},K_i} \tag{4}$$

$$X_{\text{SC}_{C_3 \text{H}_6}, i} = \left(\frac{\partial \ln S_{C_3 \text{H}_6}}{\partial \ln k_i}\right)_{k_{j \neq i}, K_i} \tag{5}$$

Experimental Details. The PdIn bimetallic catalyst was synthesized using a sequential strong electrostatic adsorption method following the procedure outlined by Wu et al. 15 First, a solution of indium(II) nitrate and citric acid in a 1:3 molar ratio was adjusted to pH 11 using ammonium hydroxide. This solution was then impregnated on Davisil 646 silica and dried at 125 °C overnight, followed by calcination at 200 °C for 3 h. Pd was added using a 10 wt % solution of palladium(II) tetraamine nitrate that had been diluted with DI water and the pH adjusted to 11 using ammonium hydroxide. The resulting sample was dried again overnight at 125 °C followed by calcination at 200 °C for 3 h. The resulting catalyst was reduced by a 2.5 °C/min ramp to 200 °C and a 10 °C/min ramp to 600 °C in a 5% H₂/N₂ atmosphere. Since the catalyst was prepared by the same synthesis method as used in our previous work, 15 the PdIn alloy composition (1:1) and the particle size distribution are also assumed to be the same. The particle size distribution of the reduced catalyst sample can be found in Figure 2 in reference 15.

The catalyst reactor setup and testing were similar to what was shown in our previous work. 10,35 In brief, catalyst reactivity testing was performed in a fixed bed microreactor setup. A total of 150 mg of catalyst was mixed with 850 mg of Davisil silica and loaded into a quartz tube reactor with an inner diameter of 9.5 mm. The catalyst was reduced in 5% $\rm H_2/N_2$ at 550 °C for 30 min after having been dried in flowing nitrogen at 100 °C for 15 min. Propane dehydrogenation was then performed at 550 °C at 3 psig in a 2.5% $\rm H_2/2.5\%$ propane/ $\rm N_2$ stream. The catalyst was exposed to this stream for 24 h until it was cooled to room temperature in flowing nitrogen and removed from the reactor for analysis. Reactivity was monitored by an online HP 6890 gas chromatogram equipped with a flame ionization detector and Restek Alumina BOND/ $\rm Na_2SO_4$ column. The reactor effluent was sampled every 5 min.

TEM images of the spent catalyst were collected by loading samples onto holey carbon grids via dry impregnation using a JEOL 2010F TEM/STEM equipped with an Oxford energy dispersive X-ray spectroscopy detector. Particle statistics were counted by analyzing images from a GATAN ES500W 27 Erlangshen wide-field camera using a Digital Micrograph from Gatan Inc., to a total count of 100 particles.

■ RESULTS AND DISCUSSION

Reaction Network. The reaction network for converting propane to propylene and deep dehydrogenation byproducts is shown in Figure 1. In the first step, propane dehydrogenates to form 1-propyl (CH₃CH₂CH₂*) or 2-propyl (CH₃CHCH₃*), either of which can undergo a second C-H bond scission to form propylene. Propylene can desorb or further dehydrogenate to form 1-propenyl (CH₃CHCH*) or 2-propenyl (CH₃CCH₂*) intermediates, which after additional dehydrogenation yield propyne. Alternatively, the propyl groups can directly form propylidene (CH₃CH₂CH* or CH₃CCH₃*) intermediates which then dehydrogenate to form 1-propenyl, 1-propylidyne (CH₃CH₂C*), or 2-propenyl. These intermediates may undergo additional dehydrogenation to produce propyne (CH₃CCH*), propynyl (CH₃CC*), or even propynlynl (CCC*), which are thought to be precursors for C-C bond scission and the formation of C₁ and C₂ species. The adsorbed C₁ and C₂ species can further hydrogenate/ dehydrogenate to form gas phase methane, ethane, ethylene, and acetylene (Figure S2), ultimately leading to coking and/or formation of unselective byproducts. This analysis represents a comprehensive PDH reaction network, and its use is motivated by the hypothesis that these additional pathways (from propynyl to propynl-ynl) may play an important role in determining the selectivity and coverages of deeply dehydrogenated species on alloy surfaces, where C-C bond scission could be hindered by the alloy promoter elements.

We denote the reaction steps that involve propane to propenyl formation as early dehydrogenation pathways, while the reactions from propenyl to prop-ynl-ynl (CCC*) are termed deep dehydrogenation pathways. We note that C–H bond breaking on the terminal CH₃ groups has not been explicitly considered for reaction intermediates in the later

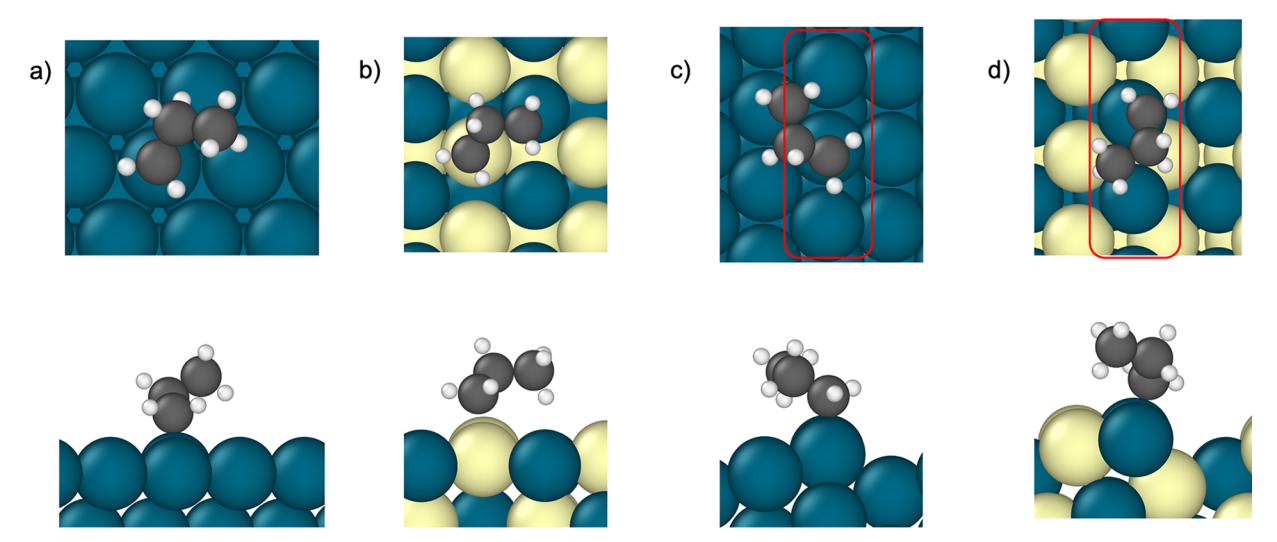


Figure 3. Top and front views of the most stable binding configurations of 1-propyl on (a) Pd(111), (b) PdIn(110), (c) Pd(211), and (d) Pd-step(210)_PdIn. The rectangle marked in red in c and d indicates where the step edge is located.

stages of the reaction network, from propylene to the propynyl (CH₃CC*) group. This simplification is motivated by fact that the hydrogen atoms present on the terminal CH₃ groups are farther from the metal surface than are the hydrogen atoms on the other carbons, and this increased distance is assumed to result in higher C-H bond breaking barriers. This assumption has been tested for selected cases, including adsorbed propylene itself on PdIn, where C-H scission in the terminal CH₃ group is found to have a barrier that is 0.4 eV higher than other C-H activation barriers in this intermediate. The reaction energies and barriers (Tables S12-S15) are calculated for all pathways in Figures 1 and S2 and are input into a microkinetic model. However, in what follows, we only describe the energetics of the pathways and reaction intermediates that are most relevant for propylene and byproduct formation. These pathways have been identified through a degree of rate and selectivity control analysis which will be discussed in the Microkinetic Modeling section.

Adsorption Energies of Reaction Intermediates. We begin with a few general observations about adsorption energy trends on Pd and PdIn alloys. The adsorption of all intermediates in the PDH reaction network is found to be weaker on the PdIn(110) terrace as compared to the Pd(111) terrace. Adsorption on the Pd-terminated step surfaces of PdIn (hereafter, Pd-step(210)_PdIn), in turn, is stronger than on any of the other PdIn steps but still weaker than on pure Pd(211) steps. For a given catalyst composition (pure Pd or PdIn alloy), the adsorption of intermediates is always stronger on steps than on the respective terrace surfaces.

Next, we describe adsorption configurations of selected reaction intermediates that are involved in either the rate- or selectivity-determining steps for propylene and byproduct formation (see section on Microkinetic Modeling), while the most stable binding energies and configurations of all intermediates are given in Tables S4–S7. We focus, in particular, on the Pd(111), PdIn(110), Pd(211), and Pd-step(210)_PdIn surfaces, with adsorption energies and geometric information on less active In-step (210)_PdIn and mixed Pd–In (321) steps reported in Tables S8 and S9.

Propylene (CH₃CHCH₂*). Propylene adsorbs in both disigma (bridge) and pi (ontop) configurations on Pd(111) (Figure 2). The bridge configuration is more stable, with an

adsorption energy of -0.77 eV, and the C–C π bond elongates from 1.34 Å in gas phase propylene to 1.45 Å upon adsorption. An experimental surface science study has shown that propylene adsorbs only in the di-sigma mode, which is in agreement with our results. ⁶² In contrast, propylene adsorption is very weak on PdIn(110) terraces (-0.07 eV). The adsorption energies on all binding sites are similar, and the C=C bond length does not change from the gas phase value upon adsorption, indicating that propylene does not interact significantly with the surface.

On pure Pd(211) steps, the most stable adsorption configuration of propylene is di-sigma along the step edge (bridge-s) with a binding energy of -0.97 eV. On Pd-step(210)_PdIn, the most stable configuration changes to ontop Pd on the step edge (ontop-s), and the binding is weakened by 0.38 eV compared to Pd(211).

1-Propyl (CH₃CH₂CH₂*). 1-Propyl is most stable on the ontop site of Pd(111) (Figure 3 and Table 2) with a binding

Table 1. Binding Energies of Representative Species on Pure Metal and Alloy Surfaces (in eV)^a

Binding Energy (eV)	propylene	1- propyl	hydrogen	propyne	carbon
Pd(111)	-0.77	0.69	-0.63	1.81	2.14
PdIn(110)	-0.07	1.34	0.04	3.59	4.09
Pd(211)	-0.97	0.59	-0.50	1.70	1.47
Pd-step (210)_PdIn	-0.59	0.87	-0.32	2.92	3.88

"The binding energies of closed shell species (propylene) are referenced to the corresponding gas phase energies, while the binding energies of open shell species (1-propyl, hydrogen, propyne, and carbon) are referenced to the corresponding gas phase species (propane, molecular hydrogen, and methane).

energy of 0.69 eV (see Table 1 for energy reference states). On PdIn(110), the adsorption energy is weakened by 0.65 eV. Interestingly, the most stable site for adsorption on the alloy surface changes to ontop-In, with the ontop-Pd site being less stable by 0.1 eV. We note that an analogous site preference has previously been predicted for PtSn₂, where adsorption is stronger on Sn as compared to Pt,²⁸ and these results suggest that, on terraces of dilute intermetallic alloys of Pt and Pd with

Table 2. Most Stable Adsorption Configurations of Representative Species on Pure Metal and Alloy Surfaces

	propylene	1-propyl	hydrogen	propyne	carbon
Pd(111) PdIn(110)	bridge physisorbed	ontop ontop- In	fcc bridge Pd—Pd	fcc bridge Pd—Pd	hcp bridge Pd—Pd
Pd(211) Pd-step (210) _PdIn	bridge-s ontop-s (Pd)	ontop-s ontop-s (Pd)	hcp-s-t bridge-s (Pd- Pd)	hcp-d-s bridge-s (Pd- Pd)	hcp-d-s bridge-s (Pd- Pd)

post-transition metals, the promoter atom has a greater affinity than Pt or Pd for early dehydrogenated species such as 1-propyl. To further test this hypothesis, the adsorption of 1-propyl has been calculated on 1:1 PdGa terrace (Figure S6). The trend is similar to the PdIn terrace, where adsorption on the Ga ontop site is found to be more stable than on the Pd ontop site by 0.2 eV.

On both of the considered step surfaces, Pd(211) and Pd-step(210)_PdIn, the most stable configuration for 1-propyl is the ontop-s (Pd). The binding energy of 1-propyl on Pd(211) is 0.59 eV, while on Pd-step(210)_PdIn, the binding is weakened by 0.28 eV.

Hydrogen (H*). Dissociated hydrogen (Figure S3) adsorbs preferentially on the bridge and 3-fold sites of Pd(111) with a binding energy of -0.64 eV. On the PdIn(110) terrace, in contrast, the hydrogen is most stable on the bridge Pd-Pd site, with a binding energy of 0.04 eV. Furthermore, on the Pd(211) step, surface hydrogen is most stable on 3-fold sites between the step edge and the terrace surface (hcp-s-t), with a binding energy of -0.50 eV. On Pd-step(210)_PdIn, hydrogen is preferentially adsorbed on the bridge Pd-Pd site along the step edge, and the binding energy of this alloy step surface is weaker by 0.18 eV compared to Pd(211).

As propylene and related reaction intermediates become more deeply dehydrogenated, differences in adsorption energies between alloy and pure metal surfaces become larger (Table 1). This trend can be attributed primarily to the lack of Pd-only threefold sites on the alloy surfaces, which are generally the preferred adsorption sites for deeply dehydrogenated intermediates. This leads to changes in most stable

configurations, which ultimately contributes to large differences in binding energies. The binding configurations of a few such intermediates, which are relevant to rate- or selectivity-determining steps, are discussed below.

Propyne (CH₃CCH*). The most stable adsorption configuration of propyne on Pd(111) is over the fcc site, with each of the bound carbon atoms located on adjacent bridge sites (Figure 4). On PdIn(110), where no threefold sites containing only Pd exist, propyne adsorbs on the bridge Pd–Pd site. The binding energy of propyne on Pd(111) is 1.81 eV, while on PdIn(110) the adsorption is weakened by 1.78 eV, which is substantially larger than corresponding differences calculated for propylene (0.69 eV).

The most stable site for propyne on Pd(211) is across the step edge (hcp-d-s) with a binding energy of 1.70 eV, while on Pd-step(210)_PdIn, adsorption is favored on the bridge site along the step edge (bridge-s). Adsorption on the alloy is weaker by 1.21 eV than on the pure Pd step. As with the terraces, the lack of Pd-only threefold sites on the alloy surfaces leads to changes in the most stable configurations which, in turn, result in large differences in the adsorption energies.

Carbon (C*). Dissociation of deeply dehydrogenated species such as propyne and propynyl leads to the formation of C₁ and C₂ species, which may act as precursors for coke formation. In particular, carbon is most stable on the hcp site (Figure S4) of the Pd(111) surface, with a binding energy of 2.14 eV (see Table 1 for energy reference states), while on PdIn(110), the most stable site is bridge Pd–Pd, with the carbon binding energy weakened by 1.95 eV. On the step surfaces of both Pd and PdIn, the most stable adsorption site of carbon is across the step edge (hcp-d-s). The adsorption energy on Pd(211) is 1.47 eV, while the binding is weakened by 2.41 eV on Pd-step(210)_PdIn. We note that these large differences in binding energies between alloy and terrace surfaces can have a significant impact on the coverages of reaction intermediates, as will be discussed further below.

In general, on the PdIn(110) surface, intermediates in the early stages of dehydrogenation tend to adsorb on both Pd and In atoms with almost equal affinity. However, as the intermediates become more deeply dehydrogenated, they

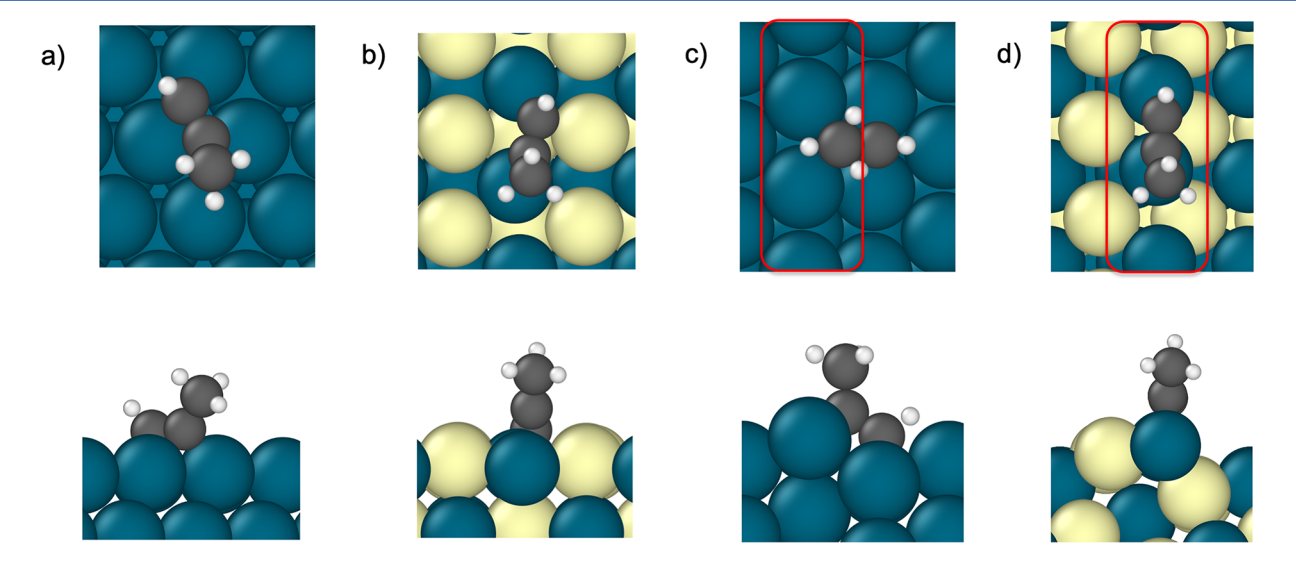


Figure 4. Top and front views of the most stable binding configurations of propyne on (a) Pd(111), (b) PdIn(110), (c) Pd(211), and (d) $Pdstep(210)_PdIn$. The rectangle marked in red in c and d indicates where the step edge is located.

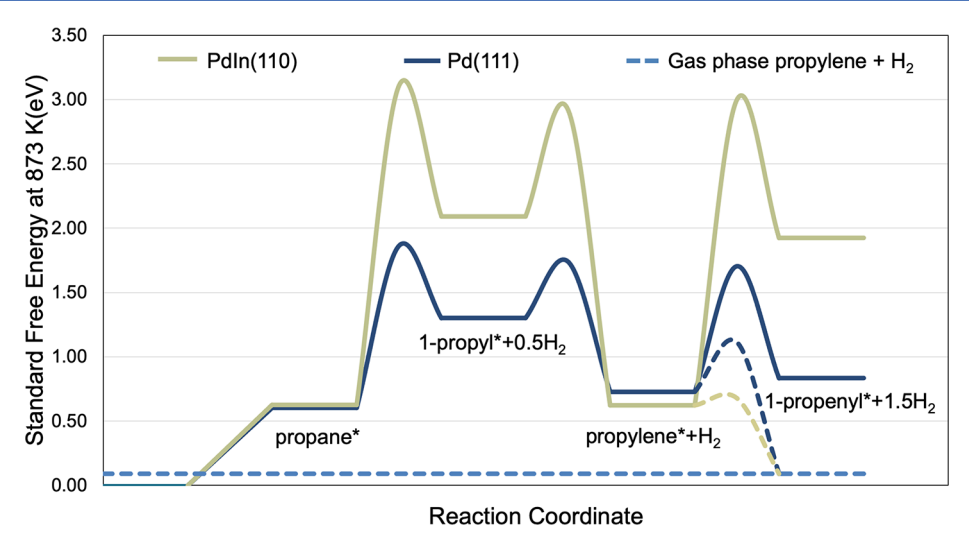


Figure 5. Standard free energy diagram at 873 K for propane dehydrogenation to form propylene, along with the subsequent deep dehydrogenation step, on Pd(111) and PdIn(110). The dotted lines represent estimated free energy barriers for propylene desorption. The free energies are referenced to the clean slabs and gas phase propane.

prefer to maximize their interaction with Pd atoms by stabilizing themselves on Pd—Pd bridge sites. These conclusions for deeply dehydrogenated intermediates are in agreement with results reported for 1:1 PdZn and PdIn terrace surfaces in our previous work.³⁵ On the other hand, on the Pd-step(210)_PdIn, all intermediates, regardless of the degree of dehydrogenation, prefer to bind to the Pd atoms along the undercoordinated edge.

Finally, to provide an electronic structure interpretation of the weakened binding energies for intermediates on the PdIn alloys, as compared to pure Pd, we perform a density of states analysis (Figure S7). The results indicate that the d-band center shifts downward in energy by 0.6 eV for Pd atoms on the PdIn surfaces compared to the Pd surfaces. These trends are in agreement with the generally accepted theory that, as the d-band center moves to the left of the Fermi level, the binding energies of intermediates become weaker. ⁶³

Standard Free Energy Analysis. Below, we first discuss activation energies and associated reaction energetics corresponding to the early dehydrogenation pathways (propane to propenyl) on both the terrace and step surfaces. Subsequently, the results for deep dehydrogenation pathways (propylene to prop-ynl-ynl/CCC*) are presented. We note that activation energy calculations have been performed for all elementary pathways discussed above (Figure 1), and the reaction energetics and barriers for all pathways are given in SI section 7. For brevity, however, only the 1-propyl (CH₃CH₂CH₂*) and 1-propenyl (CH₃CHCH*) pathways are described in detail in this section (we later demonstrate, through microkinetic analysis, that these pathways have the highest rates in the reaction network).

Early Dehydrogenation Pathway Analysis on Terraces. Figure 5 shows the standard free energy diagram for propane conversion to 1-propenyl on Pd(111) and PdIn(110) (the potential energy diagram, which includes only the DFT-calculated binding energies and barriers, is given in Figure S8). Among the reaction steps shown in Figure 5, the initial C–H bond breaking in propane has the highest free energy barriers on both PdIn(110) and Pd(111), at 2.44 and 1.26 eV, respectively. In addition to the significant potential energy barriers (1.8 eV on PdIn(110) and 0.6 eV on Pd(111)), this

reaction step also involves a substantial negative entropy change (TS ~ 0.6 eV) since a physisorbed propane undergoes dissociation to form chemisorbed 1-propyl* and H*. We note that, on Pd(111), the contribution of entropy to the free energy barriers is very small for all other reactions (0–10 J/mol-K). However, on PdIn(110), due to the physisorbed nature of propylene, the propyl to propylene formation barrier also includes a large gain in entropy (TS ~ 0.9 eV), resulting in a smaller free energy barrier.

The standard free energy diagram in Figure 5 also explicitly includes the desorption free energy barriers for propylene, which are calculated by assuming a 2-D ideal gas transition state for desorption (dotted lines in Figure 5). These barriers, in turn, permit a direct comparison between propylene desorption and dehydrogenation barriers, which is effectively an entropy-corrected variation of the traditional selectivity descriptor discussed earlier. The PdIn(110) surfaces clearly show a smaller propylene desorption barrier, as well as a larger dehydrogenation barrier, compared to Pd(111). These differences can be primarily attributed to the physisorbed nature of propylene on PdIn(110). The differences, in turn, yield selectivity descriptor values that imply higher selectivity to propylene on PdIn(110). Nevertheless, it is worth noting that, even on Pd(111), which is known experimentally to be unselective for propylene formation, 16,35 the absolute magnitude of the free energy barrier for desorption is smaller than the free energy barrier for dehydrogenation, in apparent contradiction to the experimental results. The resolution of this apparent paradox, which requires use of a more comprehensive selectivity descriptor, is discussed below in the context of the microkinetic modeling results.

For all elementary steps between propane and propenyl, activation barriers are considerably higher on PdIn(110) than on Pd(111). This result is also in tension with experimental observations, which demonstrate that turnover rates are higher on PdIn. Motivated by these considerations, and because previous studies on pure metals suggested that steps are more reactive than terraces for bond dissociation reactions, 40,64 we turn to an analysis of the kinetic barriers on step surfaces of both PdIn and Pd.

Structure Sensitivity Analysis (Early Dehydrogenation Pathways). To probe the structure sensitivity of PDH on PdIn alloys, three distinct step terminations are considered: Pd-terminated (210), In-terminated (210), and mixed Pd-In (321) (Figure 6). The surface energetics (Figure S9) of each of

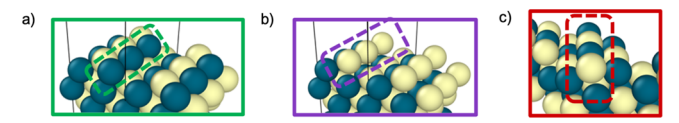


Figure 6. Three distinct step terminations on PdIn alloys: (a) Pd-step (210)_PdIn (green), (b) In-step (210)_PdIn (violet), and (c) mixed Pd—In step (321) PdIn (red)

the step terminations are found to be similar in relevant ranges of Pd chemical potentials, suggesting that any of these terminations could exist on the surface of PdIn nanoparticles, especially at high reaction temperatures (873 K). The kinetic importance of each of these structures is, therefore, evaluated by determining the dehydrogenation barriers and energetics for propane conversion to propenyl (CH₃CHCH*) and comparing to the corresponding barriers on the (110) terrace surface (Figure S10).

The dehydrogenation barriers of all the reaction steps (Figure S10) on the In-step (210) PdIn and the mixed-PdIn step (321) PdIn are similar to, or higher than, the corresponding barriers on the PdIn(110) terrace. In contrast, the free energy barriers decrease significantly (~0.6-1.3 eV) for the Pd-step(210)_PdIn compared to PdIn(110). These results suggest that the experimentally observed activity on the alloy surface can be attributed to reactions on the Pdstep(210) PdIn; this possibility will be further assessed, below, via microkinetic analysis. We note that, for the particular case of the first dehydrogenation step, which shows the highest C-H bond breaking barriers on all surfaces (Figure S10), there is a significant difference in barriers of 0.7-1.0 eV between the Pd-step and the other step terminations, even though the product propyl binding energies are within 0.2 eV of each other (Tables S7-S9). The difference in barriers is attributed to the weaker binding of H* on the In-step (210) PdIn (0.12 eV) and mixed Pd-In step (321) (-0.03 eV) terminations, in comparison to the stronger binding of H^* on Pd-step-(210_PdIn (-0.32 eV), leading to less favorable reaction energy changes and, by the BEP principle, higher activation barriers.

To compare structure sensitivity effects between the alloy and pure metal Pd, the energetics of PDH on the Pd(211) surface have also been estimated (Figure 7). The binding of all the intermediates is 0.1-0.2 eV more favorable on Pd(211) than on Pd(111), and the corresponding changes in kinetic barriers are also modest (\sim 0.1-0.3 eV). In contrast, larger changes in binding energies (0.6-1.0 eV) and free energy barriers (\sim 0.6-1.3 eV) are observed for Pd-step(210)_PdIn compared to PdIn(110) terraces. These differences clearly suggest that catalysis on PdIn and related alloys will be considerably more structure sensitive than catalysis on pure Pd, and similar conclusions are likely to apply to intermetallic alloys with intermediate compositions (for example, 3:1 Pd/In).

Finally, we briefly note that the larger difference in binding energies and activation barriers between terrace and step surfaces on the alloy, as compared to pure Pd, is in line with larger shifts in the surface *d*-band center (Figure S7). The shift in *d*-band center between Pd(111) and (211) is within 0.05 eV, while the corresponding shift between PdIn(110) and Pd-step(210) PdIn is 0.2 eV.

Deep Dehydrogenation and C–C Bond Breaking Pathways. To elucidate how unselective propylene reactions contribute to formation of byproducts and, ultimately, deactivation via coke formation, the energetics of the deep dehydrogenation pathways of propylene, and corresponding C–C bond breaking reactions, are determined on both the PdIn alloy and pure Pd (Figure 8). Given its substantially higher activity, Pd-step(210)_PdIn is the primary focus of the analysis, and binding and activation energies on this surface are contrasted with energetics of both step and terrace surfaces of pure Pd.

As mentioned above, all of the C_3 deep dehydrogenated intermediates bind more weakly on the Pd-step(210)_PdIn than on the Pd surfaces, and the difference in binding energies between the alloy and pure Pd becomes larger as propylene is successively dehydrogenated (Figure 8 and Tables S6 and S7). As a consequence, deeply dehydrogenated intermediates, such

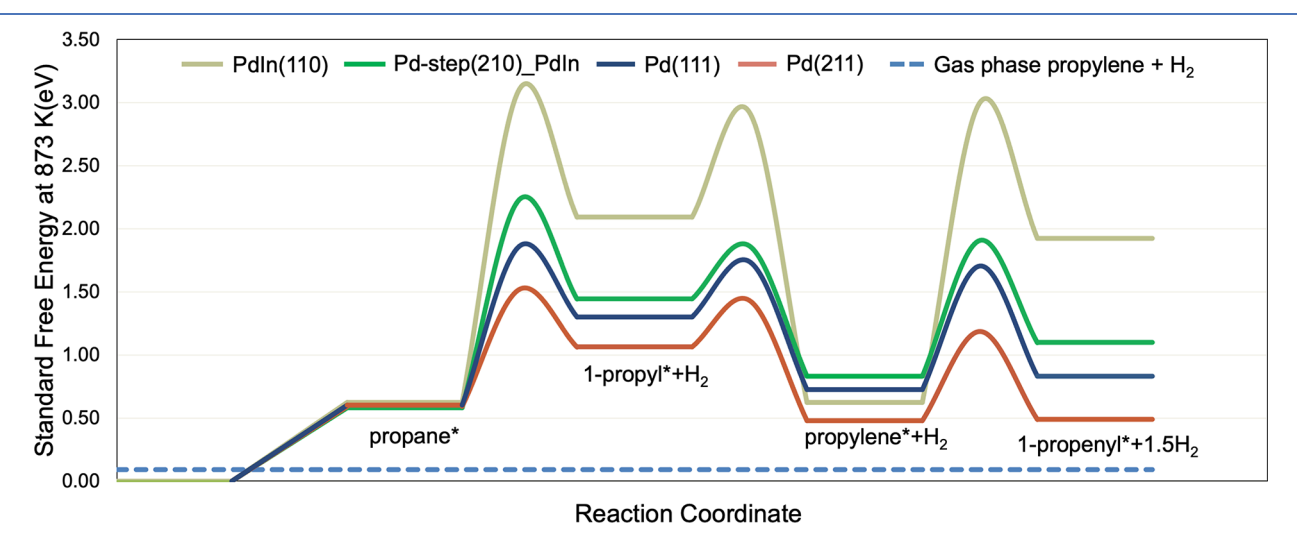


Figure 7. Propane dehydrogenation C-H bond breaking barriers on Pd(111) and PdIn(110) terraces, as well as the corresponding Pd(211) and Pd-step(210)_PdIn step surfaces. The free energies are referenced to the clean slabs and gas phase propane.

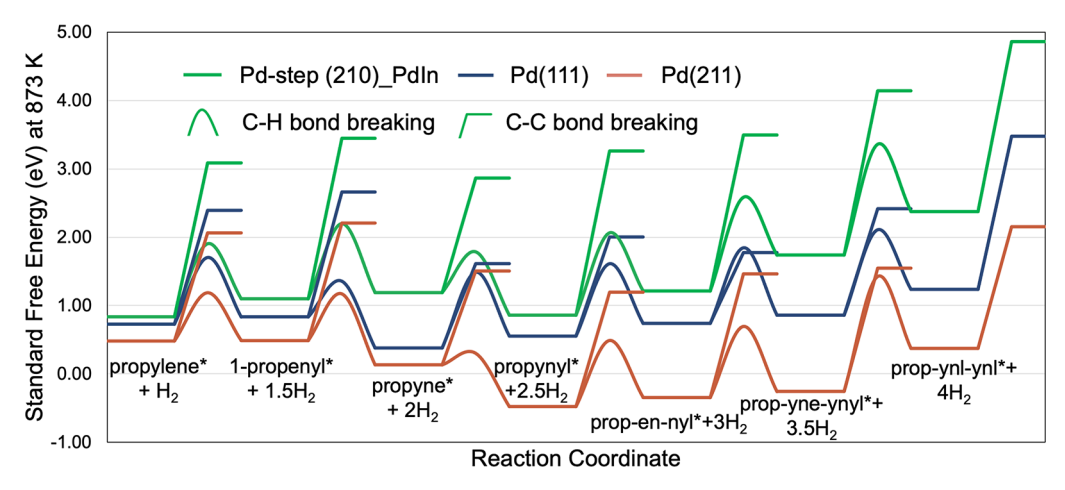


Figure 8. Free energies for deep dehydrogenation of propylene, including both C–H and C–C bond scission. The transition state free energies for C–C bond scission are represented by flat lines (the final states of the C–C bond breaking reactions are not shown for clarity). The free energies are plotted with respect to clean slab and gas phase propane references. For the chemical formula of reaction intermediates, refer to Figure 1 or Table S4.

as prop-ynl-ynl (C_3^*), are up to ~2 eV less stable on Pd-step(210)_PdIn than on Pd(211). In spite of these large thermodynamic differences, however, C–H bond breaking barriers are only ~0.2–0.5 eV higher on the Pd-step(210)_PdIn than on Pd(211). Differences in C–C bond breaking barriers between the alloy and pure Pd, on the other hand, range from 0.2 to 0.9 eV, with the larger differences generally corresponding to more deeply dehydrogenated intermediates. Similar trends are seen when comparing energetics on the Pd-step(210)_PdIn surface to those on Pd(111).

Direct comparison of C–C and C–H bond breaking barriers shows that these activation energies become comparable (within \sim 0.2 eV) for propyne (CH₃CCH*) and prop-en-ynl (CH₂CC*) intermediates on Pd(111), while the barriers have similar magnitudes at a slightly later stage of dehydrogenation, prop-yne-ynyl (CHCC*), on Pd(211). On the alloy Pd-step(210)_PdIn surface, however, the C–C bond breaking barriers are higher than C–H bond breaking barriers for all of the C₃ intermediates considered. The higher C–C bond breaking barriers, combined with the lower thermodynamic stability of the deeply dehydrogenated intermediates on Pd-step(210)_PdIn compared to pure Pd, strongly suggest that the alloy will inhibit coking and formation of C₁ and C₂ intermediates.

Before passing to a detailed discussion of gaseous byproduct formation in PDH, we note a few additional differences in C-C bond breaking chemistries between the alloy and pure metal surfaces. In general, C-C bond breaking of C₃ intermediates can occur between either the two carbon atoms bound to the surface $(\alpha - \beta)$ pathway or a surface carbon atom and a carbon atom not directly bound to the surface (β – γ pathway; Figure 9). On Pd(111), the $\alpha-\beta$ pathway has lower barriers than the β - γ pathway for all C₃ intermediates considered (Table S12). However, on Pd(211) (Table S13), both the $\alpha-\beta$ and $\beta-\gamma$ pathways have comparable barriers for 1-propenyl (CH₃CHCH*) and more deeply dehydrogenated intermediates, with the exception of propyne (CH₃CCH*). On Pdstep(210)_PdIn, the β - γ pathway is actually more favorable than the α - β pathway for adsorbed propenyl species and for more deeply dehydrogenated intermediates (Table S15). We postulate that this opposite trend for Pd-step(210) PdIn and pure Pd surfaces can be partly attributed to the highly

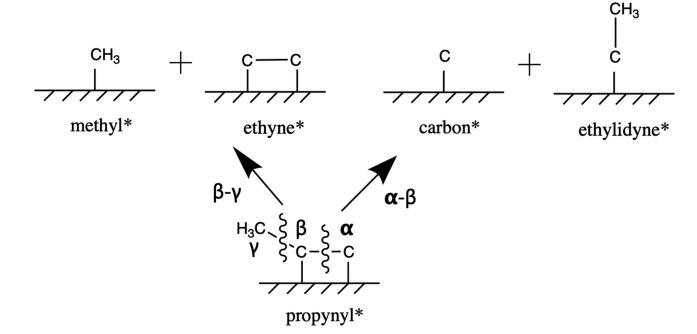


Figure 9. Two pathways through which C–C bond breaking can occur in an adsorbed propynyl intermediate.

favorable binding of methyl species, which is a product of the $\beta-\gamma$ pathway, on the step surface of the alloy, as compared to other dehydrogenated C_1 species (Figure 10).

Unselective Gas Phase Product Formation. The C_1 and C2 intermediates formed from C-C bond breaking in C3 species can further hydrogenate/dehydrogenate to form the gas phase byproducts methane, ethane, ethylene, and acetylene (Figure S2), or they may remain on the catalyst surface, ultimately leading to catalyst deactivation. To illustrate these differences, we have plotted the energetics of methane formation from carbon in Figure 10. The binding of the C₁ intermediates is weaker on the alloy surface than on pure Pd, and the weakening is enhanced for more dehydrogenated species such as carbon and methylidyne, similar to trends seen for dehydrogenated C3 intermediates in Figure 8. In fact, the overall free energy profile for methane formation on Pd(111) and Pd(211) surfaces is largely endothermic in nature (Figure 10), while it is exothermic on the Pd-step(210) PdIn surface. Similar trends in free energies are found for the C₂ intermediates (Figure S11). Hence, C1 and C2 intermediates, even if formed on the alloy surfaces, are unlikely to accumulate on the surface and will, rather, form gas phase byproducts. In contrast, pure Pd surfaces may have higher coverages of deeply dehydrogenated intermediates that poison the catalyst surface.

We briefly note that, among the C_1 intermediates, methylidyne (CH*) and carbon (C*) have the lowest free energies on Pd(111) and Pd(211), respectively, while among

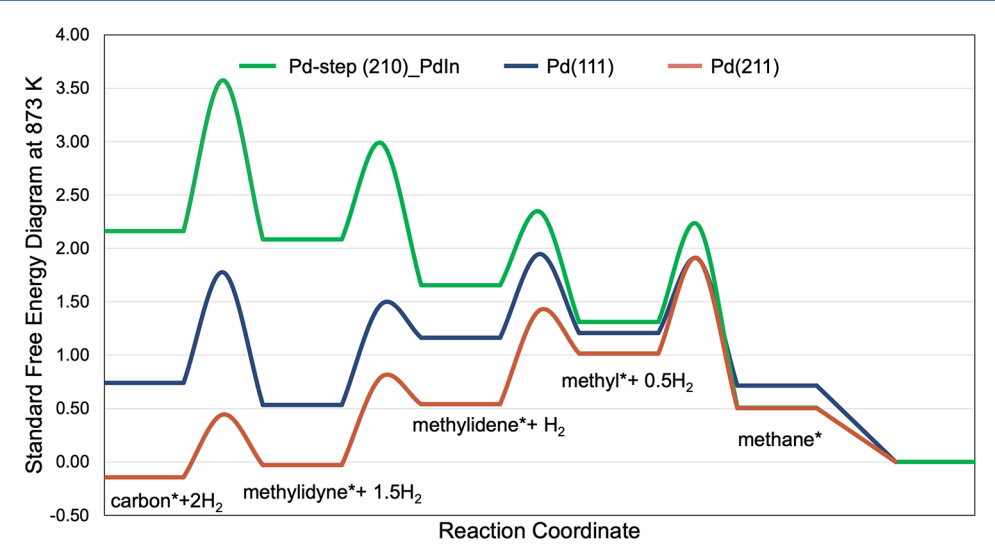


Figure 10. Standard free energy diagram for conversion of adsorbed C_1 intermediates to methane. The free energies are referenced to the clean surface and gas phase methane.

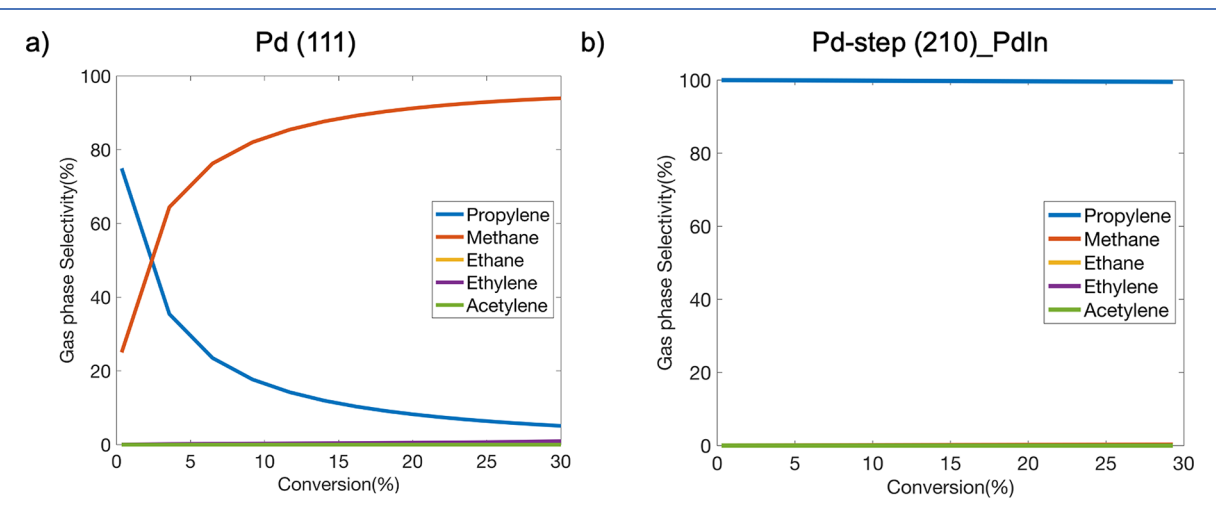


Figure 11. Selectivity of gas phase products (%) vs conversion of propane (%) at a H_2/C_3H_8 feed ratio of 1:1 on (a) Pd(111) and (b) Pd-step(210)_PdIn.

the C_2 intermediates (Figure S11), ethylidyne (CH₃C*) and ethynyl (CCH*) have the lowest free energies on Pd(111) and Pd(211), respectively. Hence, if C–C bond breaking of C_3 species occurs to a significant extent on the Pd surfaces, these intermediates will be strong candidates to be the most abundant surface intermediates (MASI). A detailed microkinetic analysis of these hypotheses is presented in the following section.

Microkinetic Modeling. In this section, we develop detailed microkinetic models of the PDH reaction network on both pure Pd and PdIn alloy surfaces. Predictions of rates and selectivities are presented at a H_2/C_3H_8 inlet feed ratio of 1:1, and the differences in coverages and dominant reaction pathways between the alloy and pure metal are analyzed at 20% conversion. These reaction conditions have been chosen to match the experimental conditions used in our previous work; 15,35 a brief discussion of the effects of different feed ratios is provided below and in SI section 12.3.

Pd(111). On Pd(111), the three significant gas phase products include methane, propylene, and ethylene (Figure 11a). As the conversion is varied from differential conversions to conversions of 30%, the selectivity to propylene decreases

from \sim 75% to 5% with a corresponding increase in methane selectivity. The decrease in propylene selectivity is associated with increased coverages of deeply dehydrogenated species (Table S19), although, at 20% conversion and hydrogen to propane feed ratios of 1:1, the absolute coverages remain quite modest. Adsorbed hydrogen has the highest overall coverage (0.12), while among the carbon-containing species, methylidyne (CH*) has the highest value (0.04).

The rates of reaction pathways that are within 2 orders of magnitude of the rate of propane adsorption are shown in Figure 12. The major pathway for propane consumption is seen to be via the 1-propyl intermediate, which then converts to adsorbed propylene. A small amount of propylene desorbs into the gas phase, but most dehydrogenates to form 1- and 2-propenyl (CH₃CHCH* and CH₃CCH₂*). These intermediates can undergo further C–H bond breaking to form propyne (CH₃CCH*), which then dissociates into adsorbed methylidyne (CH*) and ethylidyne (CCH₃*). Among all the C₃ intermediates, propyne has the highest rate of C–C bond breaking, followed by prop-en-ynl (CH₂CC*). This observation is consistent with the conclusions derived from Figure 8, where the C–H and C–C bond breaking barriers are

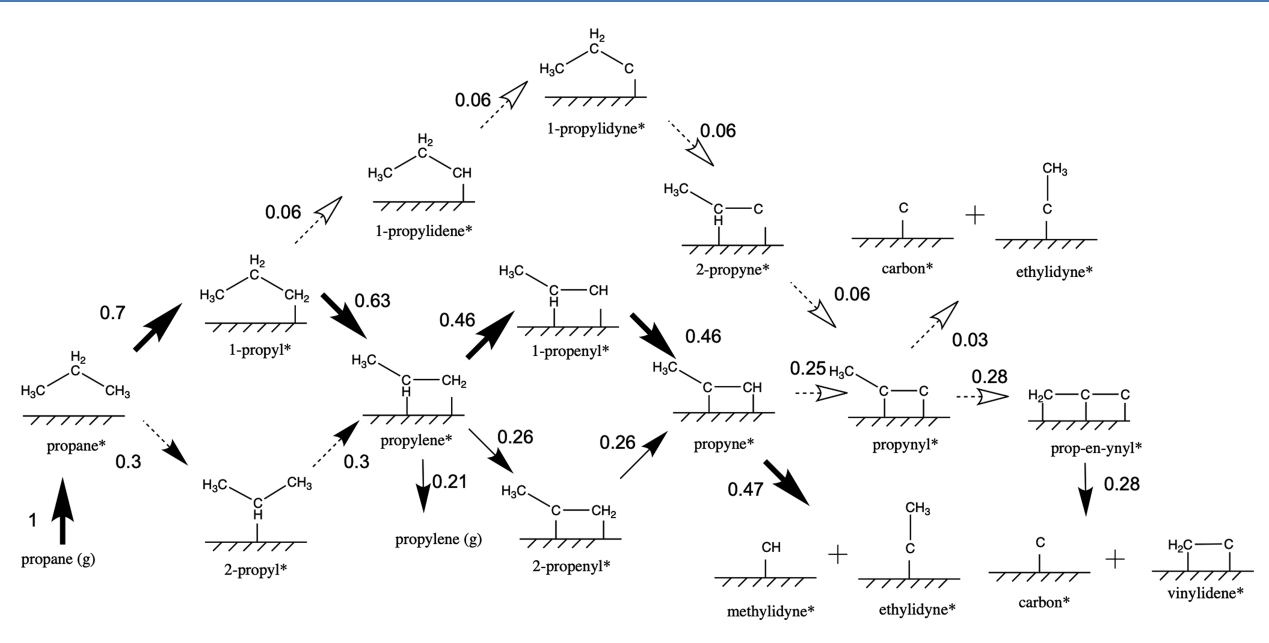


Figure 12. Dominant pathways for propylene and byproduct formation on Pd(111) at an H_2/C_3H_8 inlet feed ratio of 1:1 and 20% conversion. The net rates shown on the arrows are normalized to the rate of propane adsorption from the gas phase.

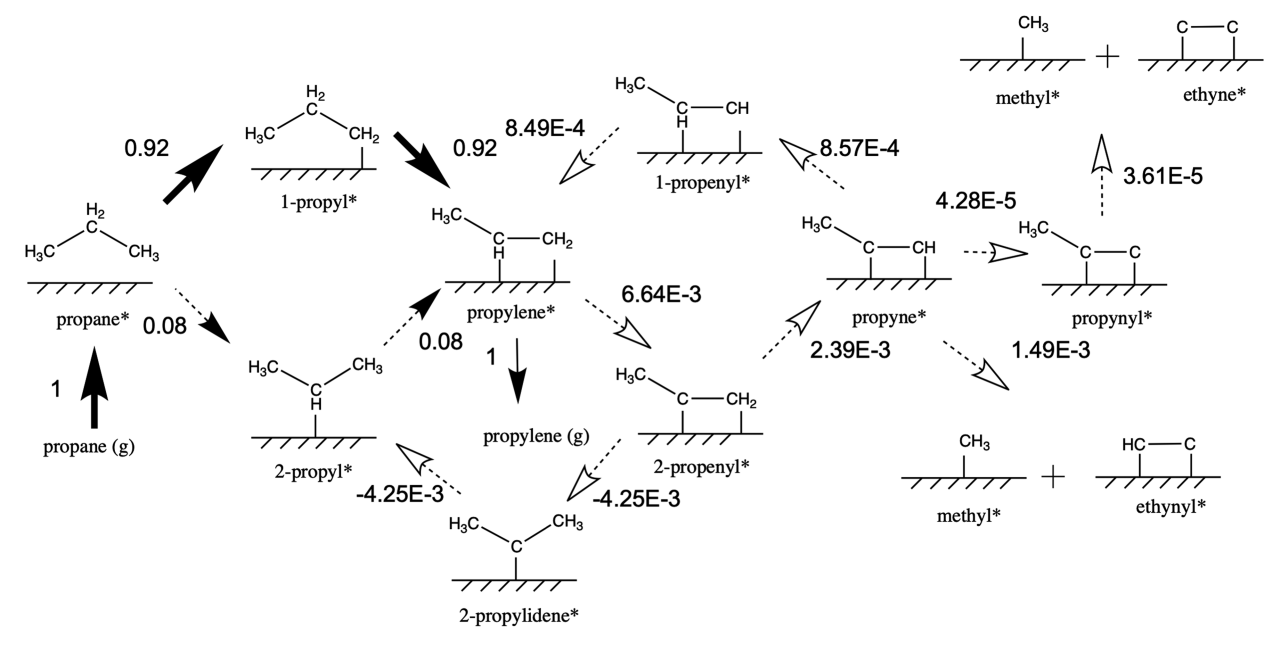


Figure 13. Dominant pathway for formation of propylene and byproducts on Pd-step(210)_PdIn at an H_2/C_3H_8 inlet feed ratio of 1:1 and 20% conversion. The net rates shown on the arrow are normalized to the rate of propane adsoption from the gas phase.

comparable for these reaction intermediates. A small fraction of propyne (CH₃CCH*) is also formed from the branching pathway of 1-propyl conversion through 1-propylidene (CH₃CH₂CH*) and 1-propylidyne (CH₃CH₂C*) intermediates.

As mentioned in the Standard Free Energy Analysis section, the barrier for the standard free energy of propylene desorption (1.11 eV) is less than the propylene dehydrogenation barrier (1.64 eV) on Pd(111) (Figure 5). However, the microkinetic results show that propylene does undergo significant dehydrogenation and consequent formation of unselective products, even at low conversions. This apparent contradiction can be understood as follows. Once propenyl (CH₃CHCH*) is formed from propylene dehydrogenation on Pd(111), it

easily undergoes further C–H and C–C bond breaking reactions to form C_1 and C_2 products, leading to a decrease in the coverages of propenyl species and, thus, irreversibly driving the propylene dehydrogenation reaction forward. However, for propylene desorption, where the desorbed propylene is in quasi-equilibrium with the propylene on the surface, there is a facile and highly reversible readsorption reaction. The quasi-equilibrated nature of propylene desorption, in contrast to the relatively irreversible propylene dehydrogenation step, leads to adsorbed propylene having higher net rates toward deep dehydrogenation pathways than desorption on Pd(111), even though the standard free energy of desorption barrier is smaller than the dehydrogenation barrier. These conclusions, which could not be obtained through inspection of the free energy

diagrams alone, highlight the importance of considering the coupled effect of rate constants and coverages via microkinetic modeling when analyzing product selectivities.

Pd(211). On Pd(211) steps, at an inlet H_2/C_3H_8 feed ratio of 1:1, the microkinetic results show that the surface is completely covered by deeply dehydrogenated C₁ and C₂ species. The most abundant surface intermediate is atomic carbon (0.61), while the intermediate ethynyl, CCH* (0.38), is also present, leading to free site coverages of only ~0.001. The higher coverages result from stronger binding of the deep dehydrogenated intermediates on the step surface (Figures 8, 10, and S11). Additionally, the high coverages result in a very low conversion (~0.2%) and effective poisoning of the step edges. We note, however, that the predicted conversions might increase modestly if adsorbate-adsorbate interactions are considered, since binding would become weaker at higher coverages. Alternatively, the carbon present on the surface could accumulate and irreversibly form coke-like species. Both of these scenarios will be analyzed in greater detail in a future study.

PdIn Alloy Surfaces. The microkinetic analyses on the terrace and step surfaces of PdIn (110 and Pd-step 210) demonstrate that the rate of propylene formation on the Pdterminated step surface is 5 orders of magnitude larger than on the terrace (Tables S22 and S23). These higher rates result from the large decrease in the activation energy barriers between the step and terrace (0.7 eV) for the initial C-H bond breaking in propane to form 1-propyl (Figure 7), which, as we demonstrate below, is the rate-limiting step for propylene formation on PdIn. Further, we note that the rate of propylene formation on Pd-step(210) PdIn is within an order of magnitude of Pd(111). The selectivity toward propylene formation on Pd-step(210) PdIn is 99% at 20% conversion, and the selectivity remains high with increasing conversion (Figure 11b), in contrast to the lower selectivities that are observed at higher conversions on Pd surfaces. These trends are consistent with the experimental observations that high selectivities are maintained at all conversions on Pd alloys. 10,15,35

As on the Pd(111) surface, the dominant pathway for conversion of propane to propylene on Pd-step(210)_PdIn is through the formation of 1-propyl (Figure 13). However, on the alloy surface, the majority of propylene desorbs into the gas phase, while only a small amount (3 orders of magnitude less) undergoes deep dehydrogenation through the 2-propenyl (CH₃CCH₂*) intermediate. The highest rates of C–C bond breaking occur in adsorbed propyne although these rates are still 3 orders of magnitude lower than the rates of propylene formation. The pathways that bypass propylene formation through 1-propylidene (CH₃CH₂CH*) and 1-propylidyne (CH₃CH₂C*) intermediates (not shown in Figure 13—see Table S23) also have very low rates on Pd-step(210)_PdIn, in contrast to what is predicted on pure Pd(111) (Figure 12), leading to even greater selectivities to propylene formation.

The calculated free site coverage on Pd-step(210)_PdIn is close to unity. This result is consistent with the experimentally observed lower deactivation rates on PdIn as compared to pure Pd. 15,35 Nevertheless, the PdIn alloy catalyst does undergo modest deactivation during time-on-stream experiments, 15,35 and, given the low adsorbate coverages, this deactivation cannot be attributed to the deeply dehydrogenated species blocking the active sites. We, therefore, hypothesize that sintering, as opposed to site blocking and coking, may be the

dominant mechanism responsible for the initially measured deactivation on PdIn alloy catalysts. To test whether sintering plays a significant role, the PdIn catalyst was exposed to propane dehydrogenation reaction conditions for 24 h and then imaged by TEM. The average particle size increased from 2 nm¹⁵ to 7 nm, which corresponds to a loss of approximately 50% total surface area of the nanoparticles (Figure S13). This result suggests that nanoparticle sintering may be a dominant mechanism of the initial deactivation for the PdIn intermetallic catalyst.

The effect of variation of inlet feed ratios on the coverages and selectivity is shown in detail in SI section 12.3. On the Pd surfaces, as the amount of H_2 in the feed increases, the coverages decrease with a concomitant decrease in selectivity toward propylene (Figure S12). These trends are in line with the recent microkinetic study on Pt surfaces by Xiao et al.³⁴ In addition, the effect of inlet feed ratios on selectivities and coverages is minimal on PdIn alloy surfaces.

Degree of Rate Control (DRC) Analysis. To determine the most kinetically significant reaction steps in the PDH reaction network, we carry out a degree of rate control and degree of selectivity control analysis for the most active facets of Pd and PdIn, Pd(111) and Pd-step(210)_PdIn. Reaction steps for which the DRC for propylene or methane formation is either greater than 0.1 or less than −0.1 are discussed in the section below (full results are tabulated in Tables S24 and S25). Methane has been chosen as a representative species for the gas phase byproducts since experiments suggest that it is one of the primary byproducts formed on all of the catalyst surfaces. ^{16−18,35}

Pd(111). The DRC analysis on Pd(111) (Table S24) shows that propane to 1-propyl conversion has the highest positive DRC (0.53) for propylene formation, while propylene dehydrogenation to form 1-propenyl (CH3CHCH*) has the highest negative DRC (-0.48). Further, closely related pathways containing isomers, including propane to 2-propyl (0.27) and propylene to 2-propenyl (-0.28), also have significant DRCs. Interestingly, even for the formation of byproduct methane, the first dehydrogenation steps (propane to 1-propyl and 2-propyl) have the highest positive DRC (0.4 and 0.18, respectively). This is a consequence of the byproducts forming from the decomposition of the desired product propylene. Additionally, the methyl (CH₃*) to methane elementary step has a positive DRC (0.16) toward methane formation, but none of the C-C bond breaking pathways have significant DRCs for this byproduct.

A degree of selectivity control analysis for propylene is also performed for all of the reaction steps (Table S24). The propylene dehydrogenation and methyl to methane steps have the highest negative values, indicating that these steps adversely affect the propylene formation selectivity. On the other hand, C–H bond breaking in propane has the largest positive degree of selectivity control, indicating that this step is ultimately responsible for propylene formation.

Pd-step(210)_Pdln. On the Pd-terminated step on PdIn, the propane to 1-propyl reaction has the highest positive DRC (0.72) for propylene formation (Table S25). All other reaction steps, including propylene dehydrogenation and C-C bond breaking, have DRCs less than 0.1 for propylene formation, reflecting the low rates of deep dehydrogenation and C-C bond breaking pathways (at least 3 orders of magnitude smaller as compared to rates of propylene formation—Figure 13). For the formation of methane, C-C bond breaking of

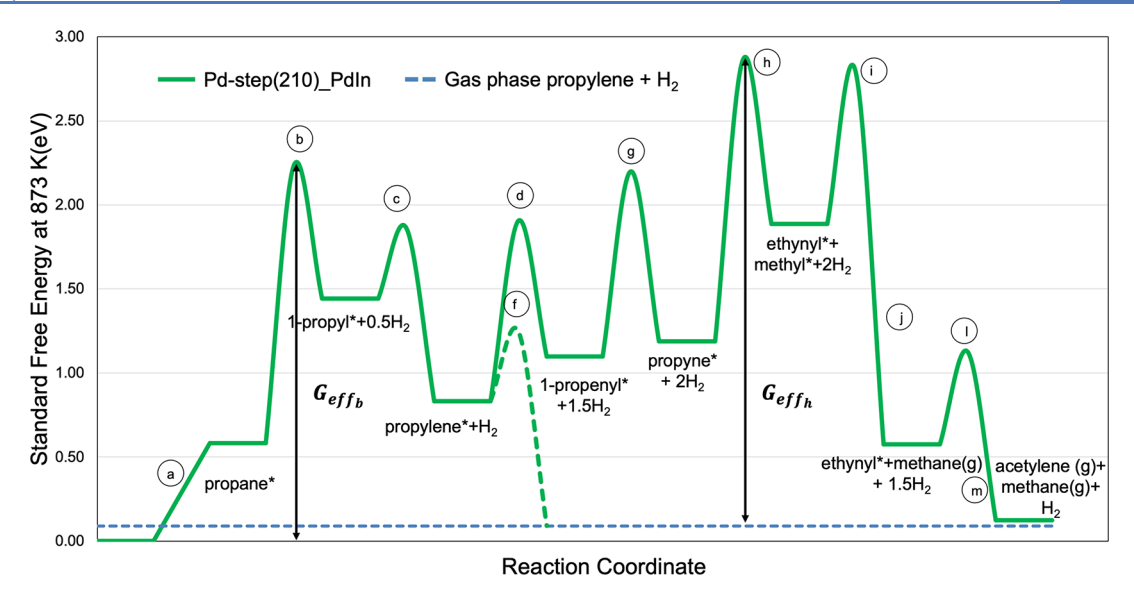


Figure 14. Standard free energy diagram of reaction steps involved in simplified rate expression analysis on Pd-step(210)_PdIn for propane conversion to propylene, as well as byproduct methane and acetylene formation. The effective activation barriers involved in the selectivity descriptor are marked as G_{eff_b} and G_{eff_b} . The green dotted line corresponds to the estimated desorption barrier for formation of propylene in the gas phase. The free energies are referenced to the clean slab and gas phase propane (g). For the chemical formulas of reaction intermediates, refer to Table S4.

propyne (CH₃CCH*) has the highest positive DRC (0.96), followed by the propane to 1-propyl step (0.59). In contrast to Pd(111), none of the propylene deep dehydrogenation steps have a significant DRC towards any of the gas phase products.

Because of the large difference in the magnitude of rates between the formation of propylene and the various by-products (Figure 13), it is difficult to evaluate a numerically meaningful degree of selectivity control for propylene formation on Pd-step(210)_PdIn. In fact, there are no numerically significant changes to propylene selectivity when the rate constants of reaction steps are varied slightly, and much larger changes (outside the range of what is normally considered for rate and selectivity control analyses) are needed to see appreciable variations.

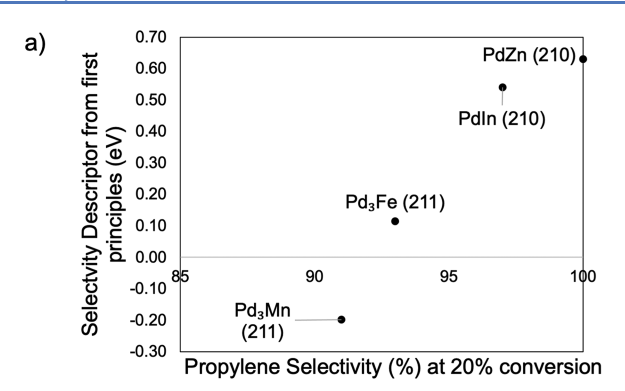
Simplified Rate Expression on Pd-step(210)_Pdln. The rates of individual steps obtained from the microkinetic model, combined with the degree of rate control analysis,

permit simplification of the overall reaction mechanism to a few kinetically significant reaction steps on Pd-step(210) PdIn. We assume that all reaction steps with DRC < 0.1 are quasi-equilibrated, while among the isomer pathways (for example, 1-propyl vs 2-propyl formation from the initial C-H bond activation in propane), only the reaction steps that have the largest rates are considered (Reaction Scheme 1). Finally, among the C-C bond breaking pathways of the reaction intermediates, only the reaction pathway for propyne (CH₃CCH*) C-C bond breaking is considered, since the rates for C-C bond breaking in propyne are found to be at least 2 orders of magnitude greater than C-C bond breaking for all other species (Figure 13). Additional details concerning the derivation of the rate expressions for gas phase propylene, and major byproducts methane and acetylene, are provided in SI section 15. The free energies corresponding to this simplified reaction mechanism are also shown in Figure 14.

Reaction Scheme 1. Reaction Steps Considered in the Reduced Reaction Mechanism for the Derivation of the Simplified Rate Expression

Using the rate expressions for gas phase products, and applying the quasi-steady state approximation for adsorbed reaction intermediates, we obtain the following expressions for propylene selectivity (eqs 6 and 7):

$$Sel = \frac{r_{C_3H_6}}{r_{C_3H_6} + r_{CH_4} + r_{C_2H_6} + r_{C_2H_4}} = \frac{1 - \frac{r_h}{r_b}}{1 + \frac{r_h}{r_b}}$$
(6)



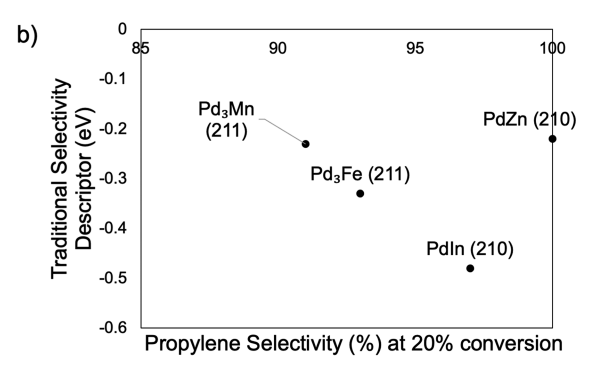


Figure 15. (a) Selectivity descriptor from first-principles $(G_{\text{eff}_h} - G_{\text{eff}_b})$ and (b) traditional selectivity descriptor (propylene desorption vs dehydrogenation) plotted against propylene selectivity at 20% conversion.

$$\frac{r_h}{r_b} = \frac{k_h K_d K_f K_g P'_{C_3 H_6} (1 - Z)}{k_b K_a P'_{C_3 H_8} K_e P'_{H_2} (1 - Q)} \sim \frac{k_h K_d K_f K_g P'_{C_3 H_6} / K_e P'_{H_2}}{k_b K_a P'_{C_3 H_8}}$$
(7)

The selectivity (eq 6) is seen to depend primarily on the rates of C-C bond breaking of propyne (r_h) and C-H bond breaking in propane to form 1-propyl (r_b) . As expected, the selectivity increases if the ratio of r_h/r_h decreases. To gain more insights into the specific kinetic and thermodynamic parameters that most impact the selectivity, we substitute the rate expressions for r_b and r_b (eqs S29 and S40), which are written in terms of forward rates multiplied by 1 minus the approaches to equilibrium for propylene (Z) and byproduct formation (Q). Since the conversions under investigation (\sim 20%) are far lower than equilibrium conversions (95%) at these conditions, the approaches to equilibrium are considerably less than unity $(Z, Q \ll 1)$. Neglecting these contributions leads to the ratio of equilibrium and rate constants, as shown in eq 7. The denominator in eq 7 corresponds to an effective barrier for the lumped reaction step of gas phase propane being converted to the transition state for C-H bond breaking of propane* to form 1-propyl* + hydrogen*, termed as G_{eff_h} (Figure 14). The numerator, on the other hand, can be interpreted in terms of an effective barrier for the lumped reaction step of gas phase propylene conversion to the transition state of C-C bond breaking of propyne (CH₃CCH*) to form ethynyl (CCH*) and methyl (CH₃*), termed as G_{eff_h} . Hence, the simplified rate expression analysis for propylene selectivity on Pd-step(210) PdIn can be interpreted as a competition between two lumped reaction steps:

$$C_3H_8(g) \to C_3H_7^* + 0.5H_2(g)$$
 (8)

$$C_3H_6(g) \to C_2H^* + CH_3^* + H_2(g)$$
 (9)

In turn, the ratio $r_{\rm h}/r_{\rm b}$ will be low if $G_{\rm eff_h}-G_{\rm eff_h}$ is very positive, thereby increasing the selectivity toward propylene formation. On the basis of this mechanistic analysis, we propose that $G_{\rm eff_h}-G_{\rm eff_h}$ can be used as a modified descriptor for selectivity, subject to the approximations described above. Moreover, the analysis implies that, in addition to the kinetic barriers associated with rate controlling steps (propane C–H and propyne C–C bond breaking), the binding energies of intermediates such as propane, propyne, and propylene are

also important for identifying the selectivity trends on alloy surfaces

The traditionally used selectivity descriptor for PDH, which compares the propylene desorption energy to the propylene dehydrogenation barrier, does not naturally appear in our revised selectivity expression. This result is, in fact, completely reasonable, given that propylene desorption is quasi-equilibrated and hence has a net rate of nearly zero, and given that the C-C bond breaking barriers of deep dehydrogenated intermediates are large compared to propylene C-H bond breaking barriers, making them rate controlling for byproduct formation (Table S25). Our revised selectivity descriptor, therefore, represents a kinetically consistent interpretation of selectivity trends that should be more reflective of the true propylene formation selectivity of Pd-containing alloys than the descriptor that has been traditionally used. However, we note that the traditional selectivity descriptor, if written in terms of a ratio of rates, becomes the rate of propylene desorption $(-r_d)$ divided by the rate of dehydrogenation (r_f) . On further simplification using the steady state approximation on surface intermediates, this ratio can be expressed as (r_b/r_h) - 1. Therefore, the $(-r_{\rm d}/r_{\rm f})$ term will be larger (more selective to propylene) if (r_b/r_h) is larger or $G_{\text{eff}_h} - G_{\text{eff}_h}$ is more positive. Hence, although there is no robust relationship between the two descriptors, predictions of qualitative trends may be similar due to the common dependence on $G_{\text{eff}_b} - G_{\text{eff}_b}$.

Finally, to evaluate the applicability of our descriptor to alloys with varying compositions, we compare the selectivity descriptor values on Pd-terminated step surfaces of four different Pd alloys, Pd₃Fe, Pd₃Mn, PdZn, and PdIn, with their experimentally determined selectivities at 20% conversion (this comparison implicitly assumes that the reaction pathways, as well as the rate determining steps, do not change across the alloy compositions). The use of Pd-terminated steps is motivated by surface energy analyses (Figure S15) showing that these step terminations are stable over chemical potential ranges that are consistent with the bulk alloy compositions. Briefly, the experiments from our previous work³⁵ have shown that 1:1 alloys, in which Pd atoms are isolated from each other, have greater selectivities than 3:1 alloys, which have threefold Pd ensembles. The descriptor values have been estimated on Pd-terminated (211) surfaces of fcc Pd₃Fe and Pd₃Mn alloys, on the (210) surface on the tetragonal PdZn, and on the (210) surface of bcc PdIn (see above results). For comparison, the traditional selectivity descriptor values (corresponding to the propylene desorption vs dehydrogenation barriers) have also been estimated on these alloy step surfaces. The corresponding binding energies and activation energies involved in estimation of the modified and traditional selectivity descriptors are given in Tables S30 and S31. For simplicity, the ZPE and standard state entropy corrections for all of the surfaces are assumed to be the same as for the Pd-terminated PdIn step surface.

Figure 15a shows the selectivity descriptor on Pd-terminated step surfaces of the four alloys plotted against selectivity at 20% conversion obtained from experiments. As mentioned earlier, the predicted selectivity will be high if the value for the modified selectivity descriptor is high (more positive). There is a clear trend of the selectivity descriptor increasing with increasing alloy composition from 3:1 alloy surfaces to 1:1 alloy surfaces, in agreement with experiments. Further, the experimental trend of PdZn having greater selectivity than PdIn is correctly predicted using the proposed selectivity descriptor. However, this is not the case with the traditional selectivity descriptor. Based on the sign convention, the predicted selectivity would be high if the traditional selectivity descriptor is more negative (Figure 15b). The trend of PdIn having greater selectivity than 3:1 alloys is correctly predicted using this approach, but the higher selectivities measured experimentally for 1:1 PdZn alloys compared to 3:1 alloys are not captured. The enhanced fidelity of the new descriptor illustrates the importance of beginning with fundamental kinetic principles to elucidate selectivity trends.

CONCLUSIONS

Using periodic density functional theory calculations and microkinetic modeling, a comprehensive reaction network for nonoxidative propane dehydrogenation is analyzed to understand the molecular features responsible for enhanced catalytic performance of bimetallic Pd alloys compared to pure metal Pd. A 1:1 alloy of PdIn is studied as a test case, where a Pdterminated step edge is found to be the most active surface feature for propane activation, with 5 orders of magnitude higher rates than PdIn terraces. On pure Pd, however, Pd(111) terraces are predicted to have considerably lower coverages of carbon-containing species and, hence, higher rates than Pd(211) step features. Analysis of deep dehydrogenation pathways on the PdIn step edge shows that the weakened binding of deep dehydrogenated intermediates, in addition to the high C-C bond breaking barriers, are responsible for the high selectivity and relative stability observed in experiments on these alloys. Degree of rate control and selectivity control analyses additionally demonstrate that, on the alloy surface, the C-C bond breaking barriers have higher DRC toward byproduct formation than do the propylene dehydrogenation pathways.

With the insights from the microkinetic analysis, a simplified expression for propylene selectivity on the PdIn step edges is developed. This expression, in turn, suggests a novel selectivity descriptor that can be expressed in terms of effective activation barriers for propyne C–C bond breaking and propane C–H bond breaking reaction steps. This selectivity descriptor is evaluated for step surfaces of four different Pd alloys. The predicted selectivity trends match well with experimentally measured selectivities on these alloys, thus underscoring how detailed microkinetic models, combined with DFT analyses, can serve as powerful tools in the identification of generalizable catalytic descriptors. The new descriptor, in turn, could find applications in screening for highly selective alloys for propane dehydrogenation.

ASSOCIATED CONTENT

Supporting Information

The Supporting Information is available free of charge at https://pubs.acs.org/doi/10.1021/acscatal.1c01916.

Binding energies and most stable site configurations of the reaction intermediates, corrections in gas phase energies, density of states analysis, reaction energetics, entropies and activation barriers of the pathways, surface energy analysis, rates and degree of rate control of reaction steps from the microkinetic modeling, derivation of simplified rate expression for selectivity descriptor, and functional dependence of binding energies (PDF)

AUTHOR INFORMATION

Corresponding Author

Jeffrey Greeley — Davidson School of Chemical Engineering, Purdue University, West Lafayette, Indiana 47907, United States; orcid.org/0000-0001-8469-1715; Email: jgreeley@purdue.edu

Authors

Ranga Rohit Seemakurthi — Davidson School of Chemical Engineering, Purdue University, West Lafayette, Indiana 47907, United States

Griffin Canning – Department of Chemical and Biological Engineering and Center for Microengineered Materials, University of New Mexico, Albuquerque, New Mexico 87131, United States

Zhenwei Wu – Davidson School of Chemical Engineering, Purdue University, West Lafayette, Indiana 47907, United States

Jeffrey T. Miller – Davidson School of Chemical Engineering, Purdue University, West Lafayette, Indiana 47907, United States; orcid.org/0000-0002-6269-0620

Abhaya K. Datye — Department of Chemical and Biological Engineering and Center for Microengineered Materials, University of New Mexico, Albuquerque, New Mexico 87131, United States; Occid.org/0000-0002-7126-8659

Complete contact information is available at: https://pubs.acs.org/10.1021/acscatal.1c01916

Notes

The authors declare no competing financial interest.

ACKNOWLEDGMENTS

This paper is based upon work supported in part by the National Science Foundation through the Center for Innovative and Sustained Transformation of Alkane Resources (CISTAR) under Cooperative Agreement No. EEC-1647722. Use of the Center for Nanoscale Materials, an Office of Science user facility, was supported by the U.S. Department of Energy, Office of Science, Office of Basic Energy Sciences, under Contract No. DE-AC02-06CH11357. Use of the National Energy Research Scientific Computing Center is also gratefully acknowledged.

REFERENCES

(1) Stangland, E. E. Shale Gas Implications for C 2 -C 3 Olefin Production: Incumbent and Future Technology. *Annu. Rev. Chem. Biomol. Eng.* **2018**, *9*, 341–364.

- (2) Sattler, J. J. H. B.; Ruiz-Martinez, J.; Santillan-Jimenez, E.; Weckhuysen, B. M. Catalytic Dehydrogenation of Light Alkanes on Metals and Metal Oxides. *Chem. Rev.* **2014**, *114*, 10613–10653.
- (3) Ding, J.; Hua, W. Game Changers of the C3 Value Chain: Gas, Coal, and Biotechnologies. *Chem. Eng. Technol.* **2013**, *36*, 83–90.
- (4) Virnovskaia, A.; Rytter, E.; Olsbye, U. Kinetic and Isotopic Study of Ethane Dehydrogenation over a Semicommercial Pt,Sn/Mg(Al)O Catalyst. *Ind. Eng. Chem. Res.* **2008**, *47*, 7167–7177.
- (5) Cybulskis, V. J.; Bukowski, B. C.; Tseng, H.-T.; Gallagher, J. R.; Wu, Z.; Wegener, E.; Kropf, A. J.; Ravel, B.; Ribeiro, F. H.; Greeley, J.; Miller, J. T. Zinc Promotion of Platinum for Catalytic Light Alkane Dehydrogenation: Insights into Geometric and Electronic Effects. ACS Catal. 2017, 7, 4173–4181.
- (6) Nakaya, Y.; Hirayama, J.; Yamazoe, S.; Shimizu, K.; Furukawa, S. Single-Atom Pt in Intermetallics as an Ultrastable and Selective Catalyst for Propane Dehydrogenation. *Nat. Commun.* **2020**, *11*, 2838
- (7) Wegener, E. C.; Wu, Z.; Tseng, H.-T.; Gallagher, J. R.; Ren, Y.; Diaz, R. E.; Ribeiro, F. H.; Miller, J. T. Structure and Reactivity of Pt—In Intermetallic Alloy Nanoparticles: Highly Selective Catalysts for Ethane Dehydrogenation. *Catal. Today* **2018**, *299*, 146–153.
- (8) Ma, Z.; Wu, Z.; Miller, J. T. Effect of Cu Content on the Bimetallic Pt-Cu Catalysts for Propane Dehydrogenation. *Catal. Struct. React.* **2017**, *3*, 43–53.
- (9) Sun, P.; Siddiqi, G.; Vining, W. C.; Chi, M.; Bell, A. T. Novel Pt/Mg(In)(Al)O Catalysts for Ethane and Propane Dehydrogenation. *J. Catal.* **2011**, 282, 165–174.
- (10) Wu, Z.; Bukowski, B. C.; Li, Z.; Milligan, C.; Zhou, L.; Ma, T.; Wu, Y.; Ren, Y.; Ribeiro, F. H.; Delgass, W. N.; Greeley, J.; Zhang, G.; Miller, J. T. Changes in Catalytic and Adsorptive Properties of 2 Nm Pt3Mn Nanoparticles by Subsurface Atoms. *J. Am. Chem. Soc.* **2018**, *140*, 14870–14877.
- (11) Hu, Z. P.; Yang, D.; Wang, Z.; Yuan, Z. Y. State-of-the-Art Catalysts for Direct Dehydrogenation of Propane to Propylene. *Chin. J. Catal.* **2019**, *40*, 1233–1254.
- (12) Pham, H. N.; Sattler, J. J. H. B.; Weckhuysen, B. M.; Datye, A. K. Role of Sn in the Regeneration of Pt/ γ -Al 2 O 3 Light Alkane Dehydrogenation Catalysts. *ACS Catal.* **2016**, *6*, 2257–2264.
- (13) Purdy, S. C.; Ghanekar, P.; Mitchell, G.; Kropf, A. J.; Zemlyanov, D. Y.; Ren, Y.; Ribeiro, F.; Delgass, W. N.; Greeley, J.; Miller, J. T. Origin of Electronic Modification of Platinum in a Pt3V Alloy and Its Consequences for Propane Dehydrogenation Catalysis. ACS Appl. Energy Mater. 2020, 3, 1410–1422.
- (14) LiBretto, N. J.; Yang, C.; Ren, Y.; Zhang, G.; Miller, J. T. Identification of Surface Structures in Pt3Cr Intermetallic Nanocatalysts. *Chem. Mater.* **2019**, *31*, 1597–1609.
- (15) Wu, Z.; Wegener, E. C.; Tseng, H.-T.; Gallagher, J. R.; Harris, J. W.; Diaz, R. E.; Ren, Y.; Ribeiro, F. H.; Miller, J. T. Pd-In Intermetallic Alloy Nanoparticles: Highly Selective Ethane Dehydrogenation Catalysts. *Catal. Sci. Technol.* **2016**, *6*, 6965–6976.
- (16) Childers, D. J.; Schweitzer, N. M.; Shahari, S. M. K.; Rioux, R. M.; Miller, J. T.; Meyer, R. J. Modifying Structure-Sensitive Reactions by Addition of Zn to Pd. *J. Catal.* **2014**, *318*, 75–84.
- (17) Yang, C.; Wu, Z.; Zhang, G.; Sheng, H.; Tian, J.; Duan, Z.; Sohn, H.; Kropf, A. J.; Wu, T.; Krause, T. R.; Miller, J. T. Promotion of Pd Nanoparticles by Fe and Formation of a Pd3Fe Intermetallic Alloy for Propane Dehydrogenation. *Catal. Today* **2019**, 323, 123–128.
- (18) Gallagher, J. R.; Childers, D. J.; Zhao, H.; Winans, R. E.; Meyer, R. J.; Miller, J. T. Structural Evolution of an Intermetallic Pd-Zn Catalyst Selective for Propane Dehydrogenation. *Phys. Chem. Chem. Phys.* **2015**, *17*, 28144–28153.
- (19) He, Y.; Song, Y.; Cullen, D. A.; Laursen, S. Selective and Stable Non-Noble-Metal Intermetallic Compound Catalyst for the Direct Dehydrogenation of Propane to Propylene. *J. Am. Chem. Soc.* **2018**, *140*, 14010–14014.
- (20) Hansen, M. H.; Nørskov, J. K.; Bligaard, T. First Principles Micro-Kinetic Model of Catalytic Non-Oxidative Dehydrogenation of

- Ethane over Close-Packed Metallic Facets. J. Catal. 2019, 374, 161–170
- (21) Xu, L.; Stangland, E. E.; Mavrikakis, M. Ethylene versus Ethane: A DFT-Based Selectivity Descriptor for Efficient Catalyst Screening. *J. Catal.* **2018**, *362*, 18–24.
- (22) Hook, A.; Massa, J. D.; Celik, F. E. Effect of Tin Coverage on Selectivity for Ethane Dehydrogenation over Platinum—Tin Alloys. *J. Phys. Chem. C* **2016**, *120*, 27307—27318.
- (23) Hook, A.; Celik, F. E. Predicting Selectivity for Ethane Dehydrogenation and Coke Formation Pathways over Model Pt—M Surface Alloys with Ab Initio and Scaling Methods. *J. Phys. Chem. C* **2017**, *121*, 17882–17892.
- (24) Wang, T.; Abild-Pedersen, F. Identifying Factors Controlling the Selective Ethane Dehydrogenation on Pt-Based Catalysts from DFT Based Micro-Kinetic Modeling. *J. Energy Chem.* **2021**, *58*, 37–40.
- (25) Wang, T.; Li, G.; Cui, X.; Abild-Pedersen, F. Identification of Earth-Abundant Materials for Selective Dehydrogenation of Light Alkanes to Olefins. *Proc. Natl. Acad. Sci. U. S. A.* **2021**, *118*, e2024666118.
- (26) Nykänen, L.; Honkala, K. Density Functional Theory Study on Propane and Propene Adsorption on Pt(111) and PtSn Alloy Surfaces. *J. Phys. Chem. C* **2011**, *115*, 9578–9586.
- (27) Nykänen, L.; Honkala, K. Selectivity in Propene Dehydrogenation on Pt and Pt3Sn Surfaces from First Principles. *ACS Catal.* **2013**, *3*, 3026–3030.
- (28) Yang, M. L.; Zhu, Y. A.; Zhou, X. G.; Sui, Z. J.; Chen, D. First-Principles Calculations of Propane Dehydrogenation over PtSn Catalysts. *ACS Catal.* **2012**, *2*, 1247–1258.
- (29) Hauser, A. W.; Gomes, J.; Bajdich, M.; Head-Gordon, M.; Bell, A. T. Subnanometer-Sized Pt/Sn Alloy Cluster Catalysts for the Dehydrogenation of Linear Alkanes. *Phys. Chem. Chem. Phys.* **2013**, 15, 20727–20734.
- (30) Saerens, S.; Sabbe, M. K.; Galvita, V. V.; Redekop, E. A.; Reyniers, M.-F.; Marin, G. B. The Positive Role of Hydrogen on the Dehydrogenation of Propane on Pt(111). *ACS Catal.* **2017**, *7*, 7495–7508.
- (31) Zha, S.; Sun, G.; Wu, T.; Zhao, J.; Zhao, Z.; Gong, J. Identification of Pt-Based Catalysts for Propane Dehydrogenation via a Probability Analysis. *Chem. Sci.* **2018**, *9*, 3925–3931.
- (32) Li, Z.; Yu, L.; Milligan, C.; Ma, T.; Zhou, L.; Cui, Y.; Qi, Z.; Libretto, N.; Xu, B.; Luo, J.; Shi, E.; Wu, Z.; Xin, H.; Delgass, W. N.; Miller, J. T.; Wu, Y. Two-Dimensional Transition Metal Carbides as Supports for Tuning the Chemistry of Catalytic Nanoparticles. *Nat. Commun.* **2018**, *9*, 5258.
- (33) Xiao, L.; Ma, F.; Zhu, Y.; Sui, Z.; Zhou, J.-H.; Zhou, X.; Chen, D.; Yuan, W.-K. Improved Selectivity and Coke Resistance of Core-Shell Alloy Catalysts for Propane Dehydrogenation from First Principles and Microkinetic Analysis. *Chem. Eng. J.* **2019**, 377, 120049.
- (34) Xiao, L.; Shan, Y.; Sui, Z.; Chen, D.; Zhou, X.; Yuan, W.; Zhu, Y. Beyond the Reverse Horiuti-Polanyi Mechanism in Propane Dehydrogenation over Pt Catalysts. *ACS Catal.* **2020**, *10*, 14887–14902.
- (35) Purdy, S. C.; Seemakurthi, R. R.; Mitchell, G. M.; Davidson, M.; Lauderback, B. A.; Deshpande, S.; Wu, Z.; Wegener, E. C.; Greeley, J.; Miller, J. T. Structural Trends in the Dehydrogenation Selectivity of Palladium Alloys. *Chem. Sci.* **2020**, *11*, 5066–5081.
- (36) Vang, R. T.; Honkala, K.; Dahl, S.; Vestergaard, E. K.; Schnadt, J.; Lægsgaard, E.; Clausen, B. S.; Nørskov, J. K.; Besenbacher, F. Controlling the Catalytic Bond-Breaking Selectivity of Ni Surfaces by Step Blocking. *Nat. Mater.* **2005**, *4*, 160–162.
- (37) Van Santen, R. A. Complementary Structure Sensitive and Insensitive Catalytic Relationships. *Acc. Chem. Res.* **2009**, *42*, 57–66. (38) Zhang, W.; Wang, H.; Jiang, J.; Sui, Z.; Zhu, Y.; Chen, D.;
- Zhou, X. Size Dependence of Pt Catalysts for Propane Dehydrogenation: From Atomically Dispersed to Nanoparticles. *ACS Catal.* **2020**, 10, 12932–12942.

- (39) Zhu, J.; Yang, M. L.; Yu, Y.; Zhu, Y. A.; Sui, Z. J.; Zhou, X. G.; Holmen, A.; Chen, D. Size-Dependent Reaction Mechanism and Kinetics for Propane Dehydrogenation over Pt Catalysts. *ACS Catal.* **2015**, *5*, 6310–6319.
- (40) Yang, M.-L.; Zhu, Y.-A.; Fan, C.; Sui, Z.-J.; Chen, D.; Zhou, X.-G. DFT Study of Propane Dehydrogenation on Pt Catalyst: Effects of Step Sites. *Phys. Chem. Chem. Phys.* **2011**, *13*, 3257–3267.
- (41) Kresse, G.; Furthmüller, J. Efficient Iterative Schemes for Ab Initio Total-Energy Calculations Using a Plane-Wave Basis Set. *Phys. Rev. B: Condens. Matter Mater. Phys.* **1996**, *54*, 11169–11186.
- (42) Kresse, G.; Hafner, J. Ab Initio Molecular-Dynamics Simulation of the Liquid-Metalamorphous- Semiconductor Transition in Germanium. *Phys. Rev. B: Condens. Matter Mater. Phys.* **1994**, 49, 14251–14269.
- (43) Kresse, G.; Hafner, J. Ab Initio Molecular Dynamics for Liquid Metals. *Phys. Rev. B: Condens. Matter Mater. Phys.* **1993**, 47, 558–561.
- (44) Kresse, G.; Furthmüller, J. Efficiency of Ab-Initio Total Energy Calculations for Metals and Semiconductors Using a Plane-Wave Basis Set. *Comput. Mater. Sci.* **1996**, *6*, 15–50.
- (45) Perdew, J. P.; Burke, K.; Ernzerhof, M. Generalized Gradient Approximation Made Simple [Phys. Rev. Lett. 77, 3865 (1996)]. Phys. Rev. Lett. 1997, 78, 1396–1396.
- (46) Blöchl, P. E. Projector Augmented-Wave Method. *Phys. Rev. B: Condens. Matter Mater. Phys.* **1994**, *50*, 17953–17979.
- (47) Kresse, G.; Joubert, D. From Ultrasoft Pseudopotentials to the Projector Augmented-Wave Method. *Phys. Rev. B: Condens. Matter Mater. Phys.* **1999**, 59, 1758–1775.
- (48) Klimeš, J.; Bowler, D. R.; Michaelides, A. Chemical Accuracy for the van Der Waals Density Functional. *J. Phys.: Condens. Matter* **2010**, 22, 022201.
- (49) Wellendorff, J.; Lundgaard, K. T.; Møgelhøj, A.; Petzold, V.; Landis, D. D.; Nørskov, J. K.; Bligaard, T.; Jacobsen, K. W. Density Functionals for Surface Science: Exchange-Correlation Model Development with Bayesian Error Estimation. *Phys. Rev. B: Condens. Matter Mater. Phys.* **2012**, *85*, 235149.
- (50) Harris, I. R.; Norman, M.; Bryant, a. W. A Study of Some Palladium-Indium, Platinum-Indium and Platinum-Tin Alloys. *J. Less-Common Met.* **1968**, *16*, 427–440.
- (51) King, H. W.; Manchester, F. D. A Low-Temperature x-Ray Diffraction Study of Pd and Some Pd-H Alloys. *J. Phys. F: Met. Phys.* **1978**, *8*, 15–26.
- (52) Methfessel, M.; Paxton, A. T. High-Precision Sampling for Brillouin-Zone Integration in Metals. *Phys. Rev. B: Condens. Matter Mater. Phys.* **1989**, *40*, 3616–3621.
- (53) Boes, J. R.; Mamun, O.; Winther, K.; Bligaard, T. Graph Theory Approach to High-Throughput Surface Adsorption Structure Generation. *J. Phys. Chem. A* **2019**, *123*, 2281–2285.
- (54) Wellendorff, J.; Silbaugh, T. L.; Garcia-Pintos, D.; Nørskov, J. K.; Bligaard, T.; Studt, F.; Campbell, C. T. A Benchmark Database for Adsorption Bond Energies to Transition Metal Surfaces and Comparison to Selected DFT Functionals. *Surf. Sci.* **2015**, *640*, 36–44.
- (55) Sheppard, D.; Terrell, R.; Henkelman, G. Optimization Methods for Finding Minimum Energy Paths. *J. Chem. Phys.* **2008**, *128*, 134106.
- (56) Henkelman, G.; Jónsson, H. Improved Tangent Estimate in the Nudged Elastic Band Method for Finding Minimum Energy Paths and Saddle Points. *J. Chem. Phys.* **2000**, *113*, 9978–9985.
- (57) Henkelman, G.; Uberuaga, B. P.; Jónsson, H. A Climbing Image Nudged Elastic Band Method for Finding Saddle Points and Minimum Energy Paths. *J. Chem. Phys.* **2000**, *113*, 9901–9904.
- (58) Henkelman, G.; Jónsson, H. A Dimer Method for Finding Saddle Points on High Dimensional Potential Surfaces Using Only First Derivatives. *J. Chem. Phys.* **1999**, *111*, 7010–7022.
- (59) Smidstrup, S.; Pedersen, A.; Stokbro, K.; Jónsson, H. Improved Initial Guess for Minimum Energy Path Calculations. *J. Chem. Phys.* **2014**, *140*, 214106.
- (60) Jmol: An Open-Source Java Viewer for Chemical Structures in 3D; Jmol Development Team, 2001.

- (61) Sprowl, L. H.; Campbell, C. T.; Árnadóttir, L. Hindered Translator and Hindered Rotor Models for Adsorbates: Partition Functions and Entropies. *J. Phys. Chem. C* **2016**, *120*, 9719–9731.
- (62) Stacchiola, D.; Burkholder, L.; Tysoe, W. T. Structure and Reactivity of Propylene on Clean and Hydrogen-Covered Pd(1 1 1). Surf. Sci. 2003, 542, 129–141.
- (63) Hammer, B.; Norskov, J. K. Theoretical Surface Science and Catalysis Calculations and Concepts. *Adv. Catal.* **2000**, *45*, 71–129
- (64) Liu, Z. P.; Hu, P. General Rules for Predicting Where a Catalytic Reaction Should Occur on Metal Surfaces: A Density Functional Theory Study of C-H and C-O Bond Breaking/Making on Flat, Stepped, and Kinked Metal Surfaces. *J. Am. Chem. Soc.* **2003**, 125, 1958–1967.